

7. SITE 1156¹

Shipboard Scientific Party²

PRINCIPAL RESULTS

Site 1156 is located on ~22-Ma seafloor west of the locus of the residual depth anomaly and 87 km south of Site 1155. It lies within Segment B5, midway between the bounding fracture zones, which are slightly farther apart (~65–70 km) than they are at Site 1155. This site, together with Sites 1155 and 1164, was intended to establish the temporal variability of the mantle source and of magmatic processes beneath Segment B5.

Hole 1156A was spudded in ~4867 m water depth and was washed through ~178 m of sediment, none of which was recovered. Rotary drilling continued the hole 11.4 m into basement, recovering 6.3 m (~55%) of pillow basalt from two lithologic units, a basalt-carbonate breccia (Unit 1) and a pillow lava (Unit 2). The breccia is composed of centimeter-sized angular fragments of moderately plagioclase-olivine phyric basalt, basaltic glass, and micritic limestone in a carbonate matrix. Some clasts are composite, made up of basalt and micritic limestone, and some display alteration halos that have been truncated during brecciation, suggesting a complex evolution. Void spaces in this coarse breccia have been filled by calcareous sediment. In places, this sediment is itself a fine, matrix-supported breccia with clasts of basalt, glass/palagonite, and preexisting micritic carbonate in a fine micritic matrix that has been veined and partially replaced by sparry calcite. Unit 2 is a sparsely to moderately plagioclase-olivine phyric pillow basalt.

Hole 1156B was washed through 181.6 m of sediment, recovering 2.3 m of siliceous pelagic clay in a single wash core. The hole continued 33.6 m into basement, and we recovered 9.9 m of basalt from a single lithologic unit. This unit is a moderately to highly plagioclase-olivine phyric pillow basalt with variable phenocryst abundances (2%–20%), even within single pieces. Lavas of this unit are slightly to moderately

¹Examples of how to reference the whole or part of this volume.

²Shipboard Scientific Party addresses.

altered to Fe oxyhydroxide and green-yellow clay with distinct alteration halos along fractures and calcite-filled veins.

Three handpicked glasses and five whole-rock powders were analyzed on board. Glasses from both holes are indistinguishable in composition, with 8.0–8.5 wt% MgO, whereas the whole rocks have significantly lower MgO contents, ranging from ~6.3 to 7.5 wt%. As at all Leg 187 sites, this difference does not appear to be attributable to crystal fractionation. Among the whole rocks, the least mobile elements (including Ti, Zr, and Y), as well as Fe, Ba, and Sr, are essentially invariant with decreasing MgO content and similar in concentration to the glasses, suggesting that MgO content decreases with increasing degree of alteration. In contrast, compatible elements (including Al, Ca, Na, Cr, and Ni) vary unsystematically with MgO in the whole rocks and differ in concentration from the glasses. The sense of these differences is consistent with variable enrichment of the whole-rock powders in olivine and/or plagioclase relative to the glass separates or their derivatives by fractional crystallization.

Unlike those of Site 1155, Site 1156 glasses are similar to those of 0- to 7-Ma Segment B5 lavas, suggesting that the more fertile mantle postulated for Site 1155 had evolved to a composition more like that of the present day during the intervening ~3 m.y. The Zr/Ba contents of Site 1156 glasses are very similar to those of transitional to Indian-type lavas from the present axis of Segment B5.

OPERATIONS

Transit to Site 1156

The fifth site of Leg 187 is 47 nmi southwest of Site 1155. As a result of adverse wind and sea conditions, the voyage to Site 1156 took about 7 hr at an average speed of 6.7 kt. At 1400 hr on 9 December, the vessel's speed was reduced to 5 kt in order to deploy the single-channel seismic (SCS) equipment. A faulty air line rendered the air gun inoperable, so only a 3.5-kHz survey was conducted. Our survey line crossed the precruise site survey track ~400 m north of the prospectus site where basement appeared to be somewhat shallower. Both SCS site survey data and the low-speed 3.5-kHz profile obtained on final approach to Site 1156 indicated basement was at ~200 m below seafloor.

Hole 1156A

When the survey was concluded at 1514 hr, we dropped a positioning beacon on the Global Positioning System coordinates at the crossing of the two survey tracks, ~400 m north of the prospectus site. Water depth was estimated with the precision depth recorder (PDR) to be 4878.4 m below the rig floor. The nine-collar bottom-hole assembly employed on the previous sites was made up with a new C-7 four-cone rotary bit. We initiated Hole 1156A with a rotary core barrel (RCB) at 2345 hr on 9 December and washed ahead to 118.2 mbsf before reaching basement. After recovering an empty wash barrel, we cored from 118.2 to 129.6 mbsf with a recovery of 55% (Table T1). We deployed fluorescent microspheres as a microbiological tracer on Core 187-1156A-3R. Because of excessive heave, we could not reach the depth attained previously, so the hole was abandoned. The drill string cleared the seafloor at 1500 hr on 10 December. We offset 200 m north of Hole 1156A to a

T1. Coring summary, Site 1156, p. 36.

location where seismic data indicated a somewhat thicker sediment cover for our next hole.

Hole 1156B

We began washing down at Hole 1156B at 1555 hr on 10 December and drilled ahead without incident to 181.6 mbsf before contacting basement ~60 m deeper than at Hole 1156A. The wash barrel from this interval contained 2.32 m of sediment. We recovered five RCBs from this hole, representing the interval 181.6–215.2 mbsf (Cores 187-1156B-2R to 6R), with about 30% recovery. When we retrieved the barrel containing Core 187-1156B-4R (196.8–205.9 mbsf), we discovered that the core liner had been jammed and severely twisted in the core barrel. To prevent a recurrence, we did not place plastic liners in the last two core barrels. We deployed another fluorescent microsphere tracer on Core 187-1156B-2R. Following the recovery of Core 187-1156B-6R, we decided that we had recovered enough material to reach our scientific objectives and to conclude operations. The bit cleared the seafloor at 0115 hr and the rotary table at 0845 hr on 12 December, completing operations at Site 1156.

IGNEOUS PETROLOGY

Introduction

Holes 1156A and 1156B were cored into igneous basement from 118.2 to 129.6 mbsf and from 181.6 to 215.2 mbsf, respectively. Hole 1156A recovered seven sections (Sections 187-1156A-2R-1 through 3R-3), penetrating 11.4 m into basement, with 6.30 m of recovered core (55.3% recovery). Two lithologic units have been assigned for this hole. Unit 1 is interpreted as a talus breccia. Clasts of basalt and palagonitized glass are present in two generations of micritic limestone matrix, suggesting that brecciation took place in two stages. The basalt clasts are moderately plagioclase-olivine phyric and are found in Sections 187-1156A-2R-1 through 2R-3. Unit 2 is a moderately to sparsely plagioclase-olivine phyric pillow basalt, found in Sections 187-1156A-2R-3 through 3R-3. Calcareous sediment, similar to that in Unit 1, fills inter-pillow spaces in some pieces (e.g., Sections 187-1156A-3R-2 [Piece 1] and 3R-3 [Piece 2]).

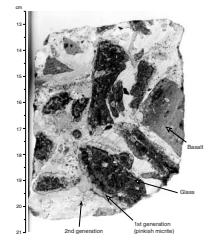
We recovered 12 sections (Sections 187-1156B-2R-1 through 6R-2) from Hole 1156B, penetrating 33.6 m into igneous basement, with 9.92 m of recovered core (29.5% recovery). About 14% of the pieces from this hole have glass rinds and/or chilled margins. All basalts were assigned to a single lithologic unit, a moderately to highly plagioclase-olivine phyric basalt.

Hole 1156A

Unit 1

The first unit is interpreted as a talus breccia. The breccia includes angular clasts of polymict slightly altered basalt, buff (where weathered) to medium gray (where fresh) (see “Alteration,” p. 5), palagonitized glass, and micritic limestone (Fig. F1). These clasts are set in a matrix of calcareous sediment composed of two types of micritic carbonate: a

F1. Basalt clasts with variably palagonitized glass in a matrix of calcareous sediment, p. 13.



pink micritic limestone and a gray micrite cement/matrix. The pink micritic limestone is present as clasts in the gray micrite and as part of some composite basalt–micritic limestone clasts. Alteration halos in some clasts have been truncated by brecciation. Both composite and truncated clasts imply that at least two stages of brecciation have taken place. Later crystalline calcite veins and patches crosscut the breccia (see “[Alteration](#),” p. 5). Clast size is highly variable, ranging from a few millimeters to several centimeters. There is no sorting either by clast size or density. The matrix is composed of gray micritic carbonate that is extensively replaced by sparry calcite. The relative amount of matrix varies from 0.5% in Section 187-1156A-2R-2 (Piece 20) to 90% in Section 2R-3 (Piece 7).

Basaltic Clasts

The angular, centimeter-sized basaltic clasts contain, on average, 4.5% phenocrysts of plagioclase and olivine, with plagioclase being the more abundant phase. The percentage of olivine and plagioclase phenocrysts varies both throughout the unit and on the scale of a single piece. In some pieces, variations in the modal percentage of plagioclase and olivine may reflect flow differentiation (e.g., Section 187-1156A-2R-2 [Piece 11]). Plagioclase is prismatic to tabular and as large as 5 mm in size. Most of the crystals are twinned and show zoning. Many plagioclase phenocrysts are partially resorbed and have irregular glassy melt inclusions. Furthermore, inclusions are concentrated at the rims of some crystals and in the interiors of others, suggesting a complex magmatic evolution. Olivine is euhedral and as large as 3 mm in size. Glassy melt inclusions up to 20 µm across are present in olivine phenocrysts from Section 187-1156A-2R-2 (Piece 15). Single- or mixed-phase glomerocrysts are present throughout the unit. In thin section, the microcrystalline groundmass texture is intersertal, with <1% olivine, 35% skeletal to prismatic plagioclase, 20% clinopyroxene sheaf quench texture, 2% opaque minerals, and 20% mesostasis (indistinguishable quench crystals + glass). Small vesicles, typically <1 mm in size, make up <1% of the rock volume. The basaltic clasts are slightly altered (see “[Alteration](#),” p. 5).

Glass/Palagonite Clasts

Subangular to rounded fragments of glass and palagonite are present within the carbonate matrix throughout the unit. They vary in size from <1 mm to several centimeters. Cross sections through palagonite rims commonly display concentric zones of alteration products of varying color ranging from yellow-cream to pink-brown (e.g., Section 187-1156A-2R-1 [Piece 8]).

Micritic Limestone

Pink micrite is present both attached to basalt clasts to form composite clasts and as smaller clasts within the gray micritic matrix (e.g., Section 187-1156A-2R-2 [Piece 4]). These micritic clasts are angular or subangular and vary in size from <1 mm to 1.5 cm. Mn oxide coatings, some with dendritic growths into the clast, are generally present. Small Mn oxide nodules are common in the micrite and may form wispy layers.

Unit 2

Unit 2 of Hole 1156A is buff (where weathered) to medium gray (where fresh), sparsely to moderately plagioclase-olivine phyric basalt.

Phenocryst abundance varies throughout the core from 3% to 8% with an average of 4%. Some pieces are highly phyric (as much as 20% phenocrysts) and display flow banding. Plagioclase phenocrysts are prismatic to tabular and as large as 6 mm. Some larger plagioclase crystals display rounded shapes, suggesting partial resorption (e.g., Section 187-1156A-3R-2 [Piece 8]). In thin section, plagioclase commonly shows partially resorbed cores overgrown by large euhedral to subhedral rims, suggesting a complex magmatic evolution (Fig. F2). Flow alignment of plagioclase is rare (e.g., Section 187-1156A-3R-1 [Piece 2]). Olivine phenocrysts are equant and as large as 4 mm. Cr spinel inclusions are present in some olivine phenocrysts (e.g., Section 187-1156A-3R-2). Glomerocrysts of plagioclase \pm olivine are rare in this unit. Near the chilled margins, the groundmass displays a sheaf quench texture. The sheafs consist predominantly of acicular to skeletal plagioclase intergrown with clinopyroxene. Otherwise, the predominant groundmass texture of the unit is intersertal. Small vesicles <0.5 mm make up ~0.5% of the rock. They are either unfilled or lined with blue cryptocrystalline silica and/or clay. Overall, the unit is slightly altered, except for Sections 187-1156A-3R-2 and 3R-3, where pieces are moderately altered (see “Alteration,” p. 5).

Hole 1156B

Unit 1

All basalt core recovered from Hole 1156B was assigned to a single lithologic unit. It is a grayish brown (where weathered) to medium gray (where fresh), moderately to highly phyric plagioclase-olivine basalt. Glass, commonly partially altered to palagonite, is present on ~14% of the pieces. Where present, glass rinds range from <0.1 to 1.5 cm in thickness. Phenocryst abundance varies from 3% for some pieces in Section 187-1156B-6R-1 to 25% for some pieces in Section 187-1156B-4R-2. Overall, the average is ~10%, of which 8% are plagioclase phenocrysts as large as 8 mm. Plagioclase varies throughout the unit from prismatic to rounded, with the larger phenocrysts tending to be rounded. In thin section, plagioclase phenocrysts are twinned and have oscillatory zoning; some have sieve-textured cores or, more rarely, aligned inclusions along cleavage or twin planes (Fig. F3). In some cases, they contain melt and fluid inclusions, but melt inclusions are more common. The average olivine phenocryst abundance is ~2%. They are equant, subhedral to euhedral crystals as large as 3 mm. Single- or mixed-phase glomerocrysts are common throughout this unit (Fig. F4).

In thin section, the groundmass is intersertal with plumose quench texture. Small spherical vesicles generally <0.5 mm in size are commonly unfilled. Overall, the unit is slightly to moderately altered (see “Alteration,” p. 5).

ALTERATION

Hole 1156A

The two basalt units recovered from Hole 1156A are generally slightly to moderately affected by low-temperature alteration. A few pieces and discrete areas within pieces are highly altered.

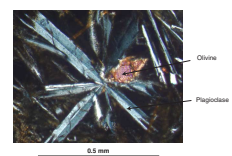
F2. A complex plagioclase phenocryst, p. 14.



F3. Sieve texture in plagioclase, p. 15.



F4. A glomerocryst of plagioclase and olivine, p. 16.



Unit 1

Unit 1 is a carbonate-cemented basalt breccia. A fundamental observation is the occurrence of at least three types of calcite: (1) the first-generation calcite is a pink micritic calcite that adheres to clasts, forming composite fragments and 0.1- to 1.5-cm angular clasts; (2) the second-generation calcite is a light gray micritic calcite (Fig. F5) forming the matrix of the breccia and surrounding the first-generation calcite; and (3) the third-generation is sparry calcite, which occurs as veins and irregular patches that may be replacement features and/or vug fillings. Throughout this chapter, we refer to these calcite varieties as first-, second-, and third-generation calcite, respectively.

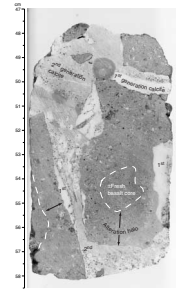
First-generation calcite is frequently separated from the adjacent basalt clast by a thin Mn oxide layer from which dendrites grow into the clast. Occasional fractures cutting basalt pieces within the breccia are filled with calcite, have Mn oxide-covered fracture walls, and are surrounded by 0.5- to 1-cm-wide oxidation halos. Vesicles are <1%, usually <<1 mm in diameter, and lined with cryptocrystalline silica. The margins of basalt clasts often have 1- to 2-cm yellowish brown oxidation halos in which olivine phenocrysts are replaced by Fe oxyhydroxide; the groundmass is mostly altered to smectite and Fe oxyhydroxide, very similar to Sites 1152 and 1154. The interiors of basalt clasts are fresher with minor smectite replacement of the groundmass (Fig. F6) and partially iddingsitized olivine (Fig. F7). The alteration halos are cut by and predate second-generation calcite veins; these veins have caused only minor (1–3 mm wide) alteration within the newly exposed basalt margins. Highly angular basalt splinters preserved within a matrix of second-generation calcite (Fig. F8) also display only minor alteration.

Crescent-shaped glass/palagonite clasts with attached first-generation calcite are enclosed by 2-to 4-mm-thick layers of yellowish to orange-brown palagonite within the second-generation calcite (Fig. F9); the centers of the larger clasts are usually fresh glass. Smaller glass clasts (0.3–1 cm) are completely altered to palagonite (Fig. F9). The thickness of palagonite encrustation is constant within each glass clast, suggesting equally intense glass alteration. This is in contrast to palagonitization of glassy pillow margins observed at the earlier sites, where palagonite dominates the outermost quench zones in layers of different thickness. Distinctive bleached whitish palagonite is occasionally present and is enclosed by a thin (<0.5 mm wide) layer of Mn oxide (Figs. F8, F10). This type of palagonite was not observed in earlier sites. The crescent-shaped glass/palagonite clasts probably represent reworked hyaloclastite, possibly filling intrapillow spaces before brecciation. The overall texture of the breccia indicates at least two brecciation events, which were accompanied by carbonate deposition and transport of smaller clasts along the opening veins.

Unit 2

Basalts of Unit 2 from Hole 1156A are slightly to moderately altered with the highest degrees of alteration within (1) veins as thick as 4 mm; (2) halos as wide as 1 cm, subparallel to the veins; (3) yellowish brown oxidation halos within the spherulitic zones of chilled pillow margins; and (4) palagonite layers within the glassy pillow rims. Veins and fractures are predominantly orthogonal to the glass rinds with smaller (<<1 mm) veins or open fractures branching off from the main veins in the vicinity of the chilled margins. Veins are generally filled with calcite

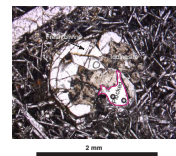
F5. Carbonate-cemented basalt breccia with two generations of calcite, p. 17.



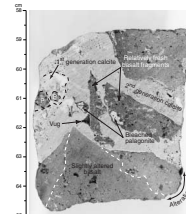
F6. Minor smectite and Fe oxyhydroxide replacement of groundmass in basalt, p. 18.



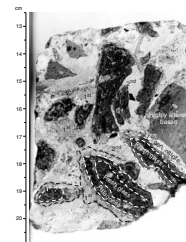
F7. Partly iddingsitized olivine phenocryst, p. 19.



F8. Crosscutting relations between first- and second-generation calcite, p. 20.



F9. Highly altered basalt and first-generation calcite clasts in matrix of second-generation calcite, p. 21.



and as wide as 4 mm (Fig. F11); fractures are covered with Mn oxide. Olivine replacement by Fe oxyhydroxide is strongest within the buff-colored halos, whereas, in the fresher medium gray areas, olivine is variably altered to a waxy yellow-green clay (smectite) along crystal outer surfaces and cracks. Although plagioclase phenocrysts appear fresh in hand specimen throughout the unit, thin-section inspection of the alteration halo in Sample 187-1156A-3R-1, 5–9 cm, reveals that plagioclase phenocrysts are in places substantially affected by iron staining along cracks and cleavage planes (Fig. F12). Groundmass plagioclase and clinopyroxene of the same section are mostly (30%–60%) replaced by smectite and Fe oxyhydroxide (Fig. F13), as is interstitial, devitrified glass. Thin-section inspection of the boundary between the alteration halo and fresh basalt in Sample 187-1156A-2R-3, 129–133 cm, reveals that the groundmass alteration grades within <0.5 mm from partially smectite/Fe oxyhydroxide replacement to virtually fresh (Fig. F14).

Hole 1156B

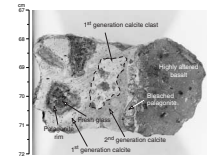
Basalt from Hole 1156B comprises a single lithologic unit that was slightly to moderately altered at low temperature. Alteration is most intense around fractures and veins and is readily apparent in hand specimen as buff-colored oxidation halos. Pieces with pervasive alteration are present in several sections (e.g., 187-1156B-2R-1, 3R-1, 3R-2, 4R-1, and 5R-1 and 187-1156A-6R-1 and 6R-2). The extent of alteration appears to be related to the high density of veins/fractures (see “**Structural Geology**,” p. 8). Several basalt fragments have smooth, weathering rinds a few millimeters thick (Section 187-1156B-4R-1); others have weathered fracture surfaces (Section 187-1156B-5R-2), suggesting that these were recovered from a talus deposit.

Veins <0.5–7 mm wide filled with calcite ± Mn oxide ± Fe-stained clay are present throughout the core. Some veins are anastomosing and/or branching and have diffuse, irregular boundaries with the host basalt (e.g., Sections 187-1156B-5R-1, 6R-1, and 6R-2). In Piece 1 of Section 187-1156B-5R-1 vein width increases downhole with a corresponding increase in width of the oxidation halos from 2–7 mm to 5–30 mm. Commonly, alteration halos are ~10 mm wide, but some are as narrow as 2 mm (e.g., Section 187-1156B-4R-3). Halo-free veins are also present (Section 187-1156B-2R-1). Open fractures are lined with Mn oxide (Sections 187-1156B-3R-2 and 6R-1) or, rarely, Fe stained with a thin coating of grayish blue silica ± spotty Mn oxide (Section 187-1156B-4R-2). Some calcite veins and fractures occur as exterior faces of pieces in Section 187-1156B-4R-3 (Pieces 2A and 2B) and in Section 5R-1. In Section 187-1156B-3R-2 (Piece 3B), a 5- to 10-mm-wide micritic calcite vein is attached with an irregular contact to basalt, and highly altered basalt pieces lined with Mn oxide are enclosed in the vein material.

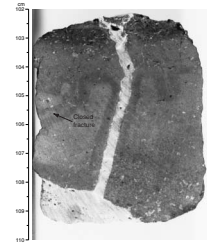
In the glassy pillow margins in Sections 187-1156B-3R-1, 4R-1, 4R-2, 6R-1, and 6R-2, yellowish brown to orange palagonite has developed along fractures and cracks in the glass. Buff alteration halos up to 2 cm wide, adjacent to the glassy margins, highlight the spherulitic and coalesced spherulitic quench zones and, in Section 187-1156B-4R-2, appear to be related to cracks/veins running parallel to the glass rind. Within these halos, 50%–100% of olivine phenocrysts are partially to completely replaced by Fe oxyhydroxide and clay ± calcite, whereas plagioclase is unaltered.

In pillow interiors, pervasive olivine alteration is also common. In Sections 187-1156B-4R-2 and 4R-3, however, olivine is unaltered or

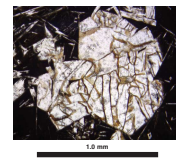
F10. Three clast types in a second-generation calcite matrix, p. 22.



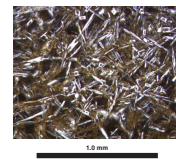
F11. Perpendicular calcite veins with alteration halos, p. 23.



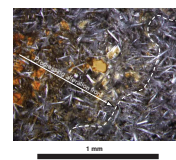
F12. Iron-stained plagioclase phenocryst, p. 24.



F13. Alteration of groundmass to smectite and Fe oxyhydroxide, p. 25.



F14. Transition from partial smectite and Fe oxyhydroxide groundmass replacement to unaltered groundmass at an alteration halo boundary, p. 26.



only partially replaced by Fe oxyhydroxide. The groundmass is variably altered, with complete to patchy replacement by a mixture of Fe oxyhydroxide and brown to greenish clay with sporadic calcite. Some pieces also show a concentric arrangement of alteration zones in which the oxidized zone forms the outer edge (e.g., Section 187-1156B-6R-2). Inside the oxidized edge is a zone in which the groundmass is replaced by clay. The interiors of these pieces are less altered but still contain some groundmass clay. The boundaries between the different clay-bearing zones are relatively sharp. Rare vesicles are empty to variably filled with clay and/or calcite; some are lined with blue to white cryptocrystalline silica. Vugs are filled with drusy calcite, and Mn oxide is present in some pieces.

MICROBIOLOGY

At Site 1156, four rock samples were collected as soon as the core liners were split to characterize the microbial community (Table T2). Three samples are pillow basalt fragments, composed of partially altered glass rinds and crystalline basalt interiors (Samples 187-1156A-3R-3 [Piece 1, 0–3 cm], 187-1156B-2R-1 [Piece 14, 93–97 cm], and 187-1156B-6R-1 [Piece 4, 50–54 cm]) and one is crystalline basalt (Section 187-1156B-5R-1 [Piece 7]). To minimize drilling-induced contamination, the outer surfaces of the rock samples were quickly flamed with an acetylene torch. Enrichment cultures and samples for DNA analysis and electron microscope studies were prepared for each sample (see “**Igneous Rocks,**” p. 7, in “Microbiology” in the “Explanatory Notes” chapter).

To examine the extent and type of contamination caused by drilling fluid, fluorescent microsphere tests were carried out for Cores 187-1156A-3R and 187-1156B-2R (see “**Tracer Test,**” p. 9, in “Microbiology” in the “Explanatory Notes” chapter and Table T2). Pieces of rock were rinsed in nanopure water, the collected water was filtered, and the filters were examined for the presence of microspheres under a fluorescence microscope. Thin sections from the inner parts of the rocks were also examined. In the thin sections, microspheres were located both in fractures and on the thin-section surfaces. All were close to the thin-section (i.e., piece) margins. Those on the surface may have been relocated by polishing. Fifteen microspheres were observed in thin sections from Core 187-1156A-3R and six from Core 187-1156B-2R.

STRUCTURAL GEOLOGY

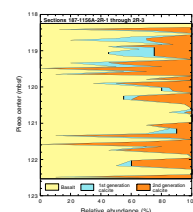
Hole 1156A

A basalt-carbonate breccia was recovered from the upper part of Hole 1156A (Core 187-1156A-2R). The breccia consists of basalt, basaltic glass/palagonite, and pink micritic calcite fragments in a light gray micritic calcite matrix, described in “**Alteration,**” p. 5, as first- and second-generation calcite, respectively. The relative abundances of basalt, first-generation calcite, and second-generation calcite in the breccia are shown in Figure F15. Calcite that fills the veins and vugs (third-generation calcite) is a minor breccia constituent and is not included in the figure.

As mentioned in “**Alteration,**” p. 5, at least two brecciation events have taken place. In some cases the second-generation calcite crosscuts

T2. Rock samples for cultures, DNA analysis, SEM/TEM, and contamination studies, p. 37.

F15. Relative abundances of basalt, pink micritic calcite, and light gray micritic calcite in breccia, p. 27.



basalt and first-generation calcite, forming a jigsaw puzzle that can be fitted together (Fig. F16). Because of this, the second brecciation may have occurred nearly in situ with little or no displacement.

The fracture + vein density and vein density for Hole 1156A average 14.8 and 4.8/m, respectively. These values are significantly lower in Core 187-1156A-2R than in Core 3R (Fig. F17). This variability reflects differences in the rock types recovered in these cores. Core 187-1156A-3R is almost exclusively basalt fragments, whereas Core 2R contains fragments of basaltic breccia with abundant matrix material (Fig. F18). The veins and fractures are much more common in basalt fragments than in breccia matrix.

Hole 1156B

Fractures and veins are the principal structures developed in basalts from Hole 1156B. Their distributions are uneven, and they are concentrated in some pieces or in Sections 187-1156B-4R-2 (Piece 1), 5R-1 (Piece 1), and 6R-1 (Pieces 1 and 7). The fracture + vein density ranges from 2.4 to 29.1/m and averages 15.2/m (Fig. F17). The vein density ranges from 1.5 to 26.2/m and averages 10.4/m. The calculated volume percent of veins ranges from 0.04 to 1.96 and averages 0.86.

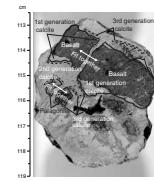
SITE GEOPHYSICS

Site selection for Site 1156 was based on a SCS survey conducted during the *R/V Melville* cruise Sojourner 5 in 1997. The proposed site is near shotpoint 270 of the seismic profile (Fig. F19). This migrated seismic profile shows clear sediment cover from 6.5- to 6.65-s two-way travel-time, giving an estimated sediment thickness of ~150 m. No presite SCS survey was conducted, owing to equipment failure. A 1.2-hr 3.5-kHz PDR survey with average ship speed of 5.0 kt was performed on the approach to Site 1156 to confirm the site location and sediment thickness. Hole 1156A is ~400 m north of prospectus site AAD-34a. Hole 1156B is 200 m farther north (see Fig. F20). The drilled sediment thicknesses were 118.2 m for Hole 1156A and 181.6 m for Hole 1156B.

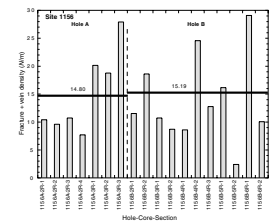
SEDIMENTS

We recovered one wash core from Hole 1156B (Core 187-1156B-1W; 0.0–181.6 mbsf). However, since hole conditions allowed no new penetration into basement at Hole 1156A (see “Operations,” p. 2), we had moved to Hole 1156B without retrieving the core barrel. There is no way to determine if the material recovered in the wash barrel was from Hole 1156A, 1156B, or both. All the sediment recovered in the wash barrel is siliceous pelagic clay, with no evidence of calcareous material. Most is pervasively drilling disturbed, but an interval near the top of Core 187-1156B-1W is packed medium dark brown clay. In Section 187-1156B-1W-1, there are three irregularly shaped pieces, several centimeters in size, of clay in varying colors embedded in the dark brown clay matrix. From 35 to 38 cm is a dark grayish brown subangular fragment of indurated clay. From 39 to 42 cm is an oblate spheroid of light brown clay, and from 47 to 52 cm is a ball of very dark grayish brown clay. A smear slide from the matrix contains brown clay, rare 2- to 10- μ m fragments of subangular to subrounded brown, translucent volcanic glass;

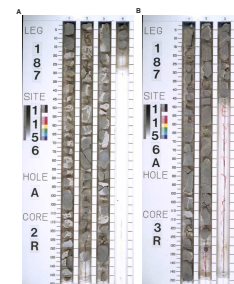
F16. Breccia fragments can be fitted together in places, p. 28.



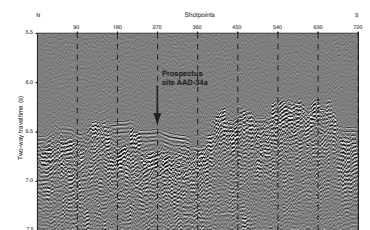
F17. Plot of fracture + vein density, p. 29.



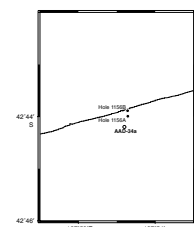
F18. Photos of Cores 187-1156A-2R and 3R, p. 30.



F19. Seismic profile crossing the general location of Site 1156, p. 31.



F20. Part of the track of the JR PDR west-to-east survey line S4, p. 32.



40- μm laths of plagioclase; and smaller ($\sim 20\ \mu\text{m}$) shards of colorless, low-birefringent minerals. There are also abundant fragments of siliceous microfossils. A smear slide from the light brown ovoid clay interval contains very light brown to colorless clay-sized fragments, rare 40- μm fragments of brown volcanic glass, and 10- μm colorless but highly birefringent crystal shards. A smear slide from the very dark grayish brown sphere of embedded clay contains brown clay, abundant siliceous microfossil fragments, and rare brown volcanic glass shards up to 90 μm across.

All of Section 187-1156B-1W-2 is soupy to highly drilling disturbed, but the matrix is similar in appearance to the dark brown clay matrix in Section 187-1156B-1W-1. There are abundant millimeter-sized pellets of clay. From 25 to 29 cm is a light-brown ball of clay similar in appearance to the light-brown ovoid interval in Section 187-1156B-1W-1. From 56 to 60 cm in Section 187-1156B-1W-2 is an interval with abundant millimeter-sized basaltic fragments. These fragments become less abundant toward the bottom of the section (93 cm).

Five pieces of basalt of unknown origin were also recovered in the wash barrel. Two small pieces at the top of the core must be retained from Hole 1156A since there were no drilling indications of hard material as we washed through the sediments at Hole 1156B. Three pieces of basalt with variable phenocryst modes were recovered from the bottom of the core barrel. One of these pieces had a veneer of lithified sediment similar to material recovered from Hole 1156A (see “[Igneous Petrology](#),” p. 3), but similar lithologies were also recovered from Hole 1156B. Although it seems likely that these are from Hole 1156B, we cannot be certain that the entire wash core is not from Hole 1156A.

GEOCHEMISTRY

Introduction

Site 1156 basalts were recovered from two holes that sampled ~ 22 -Ma crust formed within Segment B5 of the Australian Antarctic Discordance (AAD), ~ 87 km south of Site 1155. Five whole-rock powders were analyzed for major and trace elements by X-ray fluorescence (XRF) and inductively coupled plasma–atomic emission spectrometry (ICP-AES), and three glasses were analyzed by ICP-AES only. Three lithologic units, two in Hole 1156A and one in Hole 1156B, are represented by glass and whole-rock analyses (see Table T3). ICP-AES Ni and Cr results are consistently lower than those from XRF. There is also a significant analytical discrepancy in MgO and K₂O for Sample 187-1156A-2R-3 (Piece 17, 129–133 cm). The reason for the latter discrepancies is unknown; however, we conclude that the ICP-AES analysis is aberrant because the MgO and K₂O contents for Sample 187-1156A-2R-3 (Piece 17) differ from those in the remaining three Unit 1 whole-rock compositions.

Hole 1156A

Hole 1156A basalts are derived from two lithologic units, based on macroscopic and microscopic examination (see “[Igneous Petrology](#),” p. 3). Unit 1 is interpreted as a talus breccia composed of basalt clasts and palagonitized glass in a matrix of micritic limestone. Unit 2 is a moderately to sparsely plagioclase-olivine phyric pillow basalt underlying Unit 1. One glass and two whole rocks from Unit 1, as well as one

T3. Compositions of basalts, Site 1156, p. 38.

glass and one whole rock from Unit 2 were analyzed, and the results cover a substantial MgO range (6.5–8.3 wt%). As observed at previous sites, the glasses have higher MgO contents than the associated whole rocks, although the difference is only ~0.5 wt% in most cases. The two units differ in their whole-rock compositions; however, the glasses from both units are virtually identical in composition. Glass within the Unit 1 breccia may, therefore, have been derived from Unit 2 pillow rims. Unit 1 and Unit 2 whole rocks do not lie on simple fractional crystallization trends that stem from the Hole 1156A glasses. For example, Fe₂O₃ decreases with decreasing MgO; Al₂O₃, CaO, and Ni contents are high in Unit 2, consistent with the observed presence of plagioclase and olivine phenocrysts. Unit 1 whole rocks are similar to the glasses, but Fe₂O₃ and Na₂O contents should be higher in these samples if they were related by simple low-pressure crystal fractionation to a parental magma represented by Hole 1156A glass compositions.

Hole 1156B

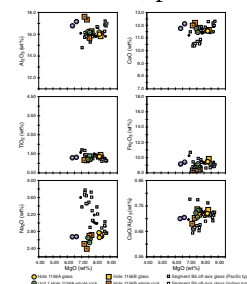
Hole 1156B basalts are assigned to a single lithologic unit of moderately to highly plagioclase-olivine phyric pillow basalt with calcareous sediment locally filling interpillow spaces (see “Igneous Petrology,” p. 3). The Hole 1156B glass is compositionally the same as Hole 1156A glasses within analytical uncertainties. Two different whole-rock compositions are evident in Hole 1156B: one similar to Hole 1156A (Unit 1) and one that could easily be related to Hole 1156A (Unit 2) by simple low-pressure crystal fractionation (i.e., decreasing Al₂O₃, CaO, CaO/Al₂O₃, Ni, and Cr and increasing Na₂O, Fe₂O₃, Sr, and Ba).

Temporal Variations

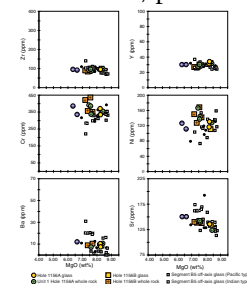
The compositional characteristics of Site 1156 lavas are compared with those of the present Segment B5 axis and off-axis lavas in Figures F21 and F22. Site 1156 glasses lie at the high-MgO end of the range for 0- to 7-Ma AAD mid-ocean-ridge basalts (MORBs). For most elements, Site 1156 glasses overlap younger Segment B5 compositions. Notably, however, Na₂O content is slightly lower in Site 1156 glasses and appreciably lower in whole rocks relative to younger lavas. The Na₂O variations in the whole rocks are orthogonal to those observed in the glass compositions and decrease with decreasing MgO. All other trends appear reasonably similar to younger Segment B5 glasses. Progressive loss of MgO from the whole rocks through alteration would be the simplest explanation for this unusual Na₂O variability.

Overall, no clear difference in source conditions (i.e., melting or composition) can be determined between Site 1156 and the near-axis Segment B5 compositions. In contrast, comparison with the data from Site 1155 (see “Geochemistry,” p. 9, in the “Site 1155” chapter), which is also located in Segment B5, shows that the Site 1156 glasses have lower Na₂O, slightly lower TiO₂ and Fe₂O₃, as well as higher Al₂O₃ and CaO for a given MgO content. Therefore, melting conditions and/or the source composition that existed beneath the Southeast Indian Ridge (SEIR) when Site 1155 lavas erupted must have changed to the parameters that now exist beneath 0- to 7-Ma crust by the time Site 1156 lavas erupted (i.e., over a period of ~3 m.y.).

F21. Major element compositions vs. MgO of basalts from Holes 1156A and 1156B, p. 33.



F22. Trace element compositions vs. MgO of basalts from Holes 1156A and 1156B, p. 34.



Mantle Domain

The Zr/Ba systematics of Site 1156 suggest an Indian-type to transitional mantle source. Glass and whole-rock compositions lie well within the range of known Indian-type MORB glasses from the SEIR (Fig. F23A). They are very similar to the Segment B5 axial samples, which are transitional between present-day Pacific type (eastern Segment B5) and Indian type (western Segment B5). As in Hole 1155B (see Fig. F23), the glasses and associated whole rocks define a coherent negative Zr/Ba vs. Ba trend. Site 1156 and Hole 1155B lavas have the same Zr/Ba range, but Site 1156 compositions have slightly higher Ba contents at a given Zr/Ba, suggesting a slightly greater contribution of Pacific-type mantle to 1156 lavas.

Similar conclusions can be drawn from the Na₂O/TiO₂ vs. MgO diagram (Fig. F23B). Most Site 1156 lavas have a slightly lower Na₂O/TiO₂ value for a given MgO content relative to the Segment B5 axial lavas, which could indicate a slightly greater Pacific-type mantle contribution. Site 1156 whole rocks have higher Na₂O/TiO₂ relative to their associated glasses, similar to the whole rocks from Site 1155. They overlap the Pacific-type Segment B5 on-axis mixing line, shown by the gray shaded line (Fig. F23B), but in contrast show little variation in Na₂O/TiO₂ with decreasing MgO. Although Na₂O/TiO₂ suggests a Pacific-type parentage for Site 1156 lavas, this suggestion would be more convincing if these samples had either higher Ba contents and/or higher Zr/Ba values. Note that lavas with Zr/Ba >14 at Ba <10 ppm can be Pacific type, transitional type, or Indian type but that no 0- to 7-Ma Pacific-type lavas have Zr/Ba <14 in this Ba-concentration range. Based on their low Zr/Ba and low Ba content, we can best conclude that the basalts from Site 1156 are derived from Indian-type mantle with some tendency toward transitional characteristics.

F23. Variations of Zr/Ba vs. Ba and Na₂O/TiO₂ vs. MgO for Hole 1156A and 1156B glass and whole rocks, p. 35.

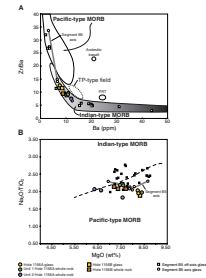


Figure F1. Photograph of Section 187-1156A-2R-2 (Piece 4), showing basalt clasts with variably palag-onitized glass in a matrix of calcareous sediment.

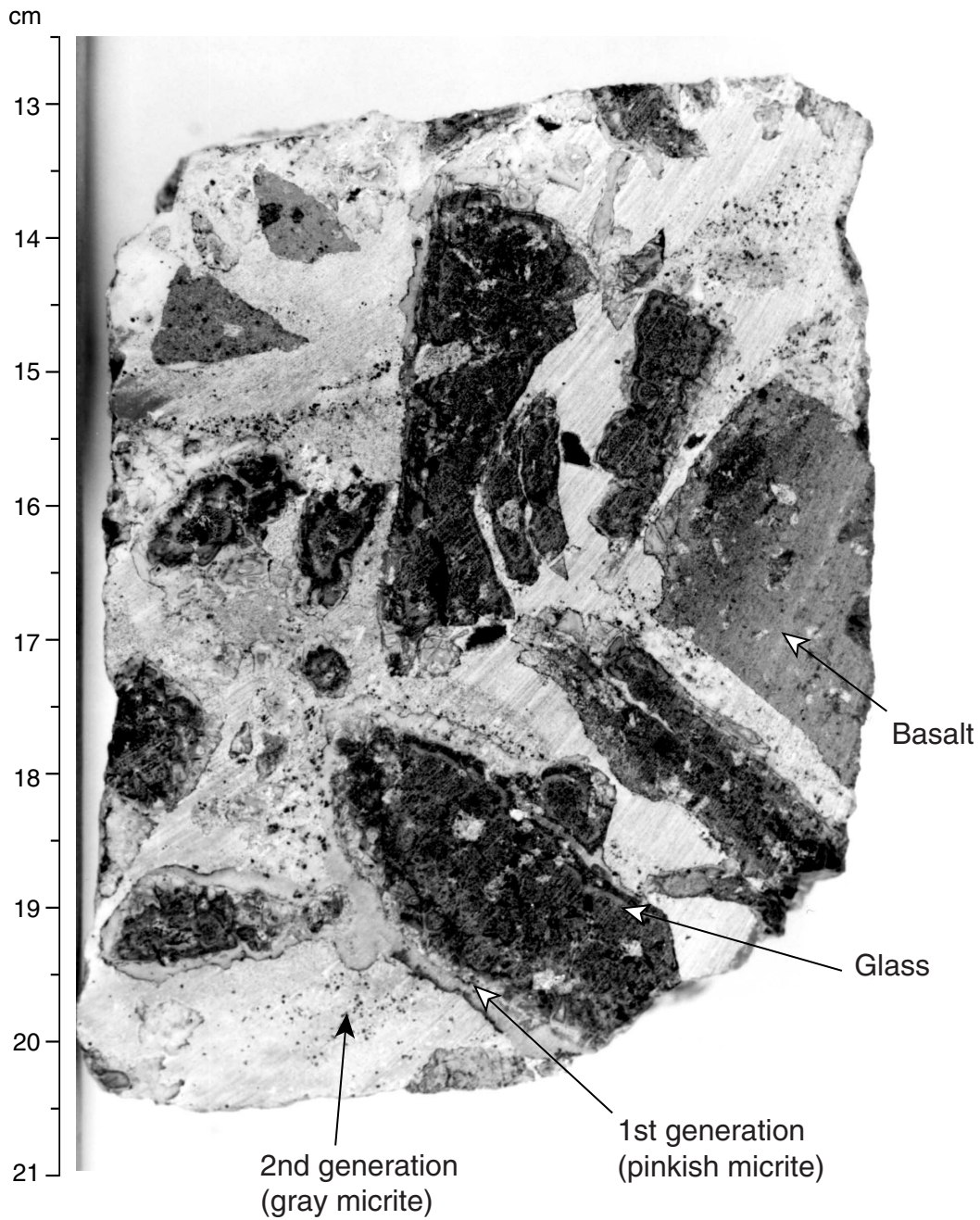
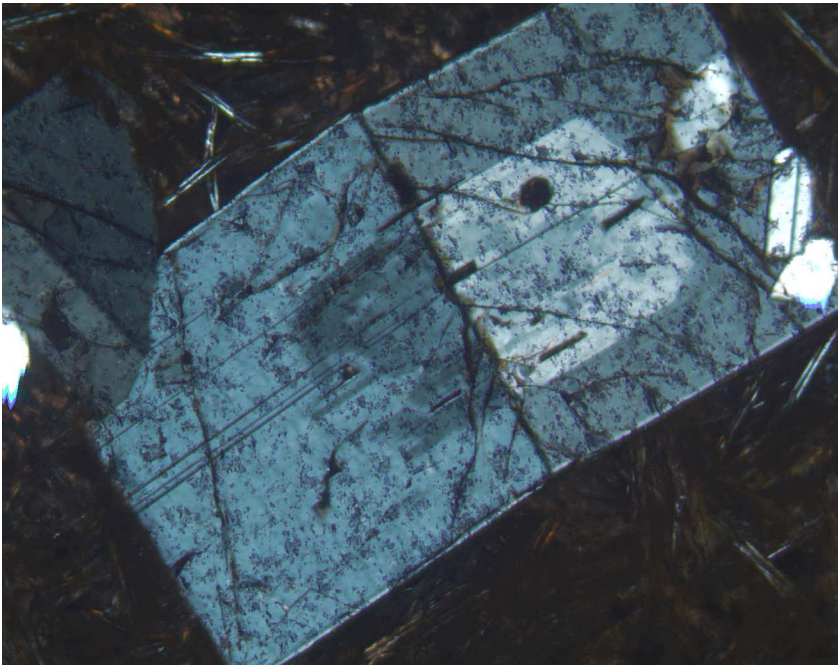


Figure F2. Photomicrograph, with crossed polars, of Sample 187-1156A-3R-2, 73–77 cm (see “[Site 1156 Thin Sections](#),” p. 26), showing a complex plagioclase phenocryst. A partially resorbed core is overgrown by a large euhedral rim, which included several small subhedral plagioclase crystals during growth.



1.0 mm



Figure F3. Photomicrograph, with crossed polars, of Sample 187-1156B-3R-1, 80–84 cm (see “[Site 1156 Thin Sections](#),” p. 27), showing sieve texture in plagioclase crystals.



2 mm



Figure F4. Photomicrograph, with crossed polars, of Sample 187-1156B-3R-1, 80–84 cm (see “[Site 1156 Thin Sections](#),” p. 27), showing a glomerocryst of plagioclase and olivine.

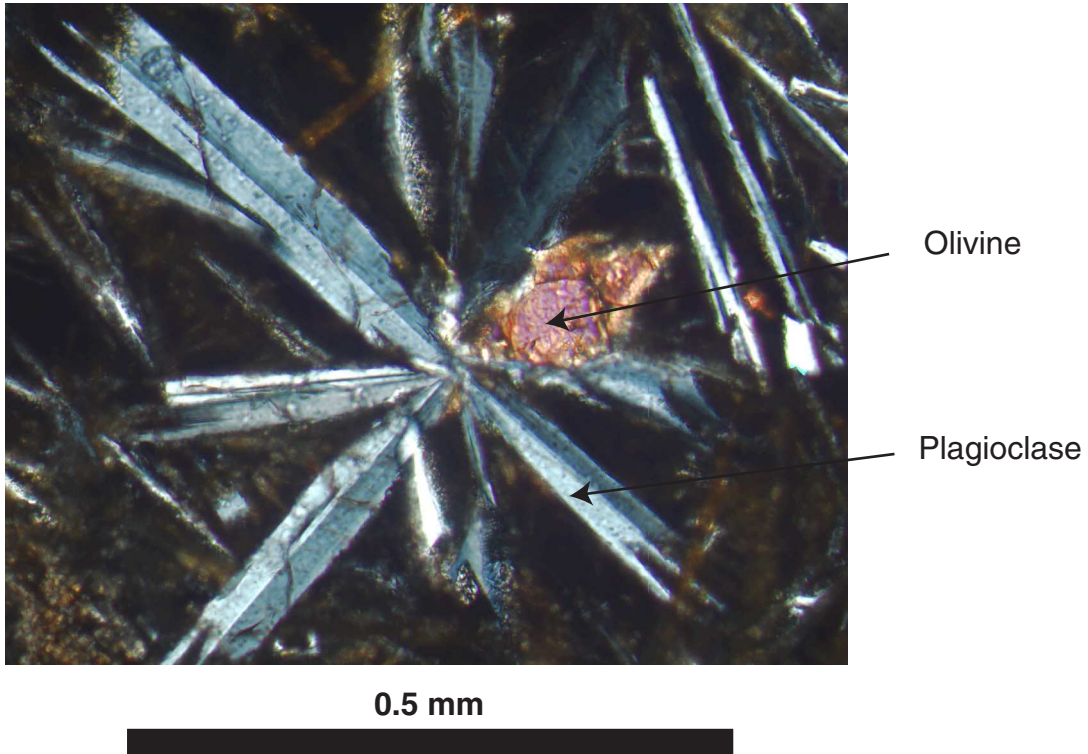


Figure F5. Photograph of interval 187-1156A-2R-2W, 47–58 cm, showing carbonate-cemented basalt breccia. Pink micritic carbonate (first-generation calcite) is attached to large basalt clasts and is also present as angular pieces within the matrix of light gray micritic (second-generation) calcite.

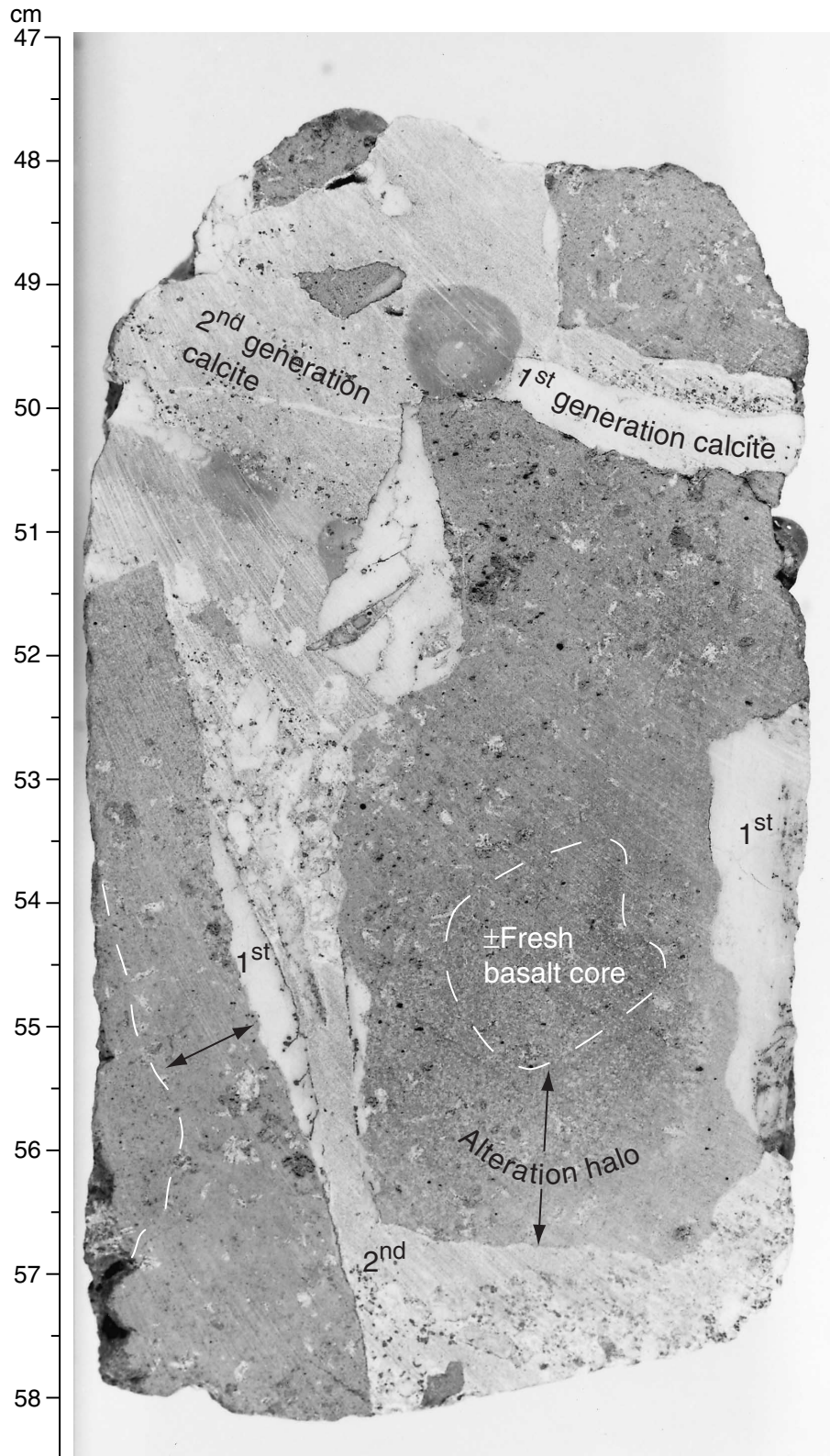
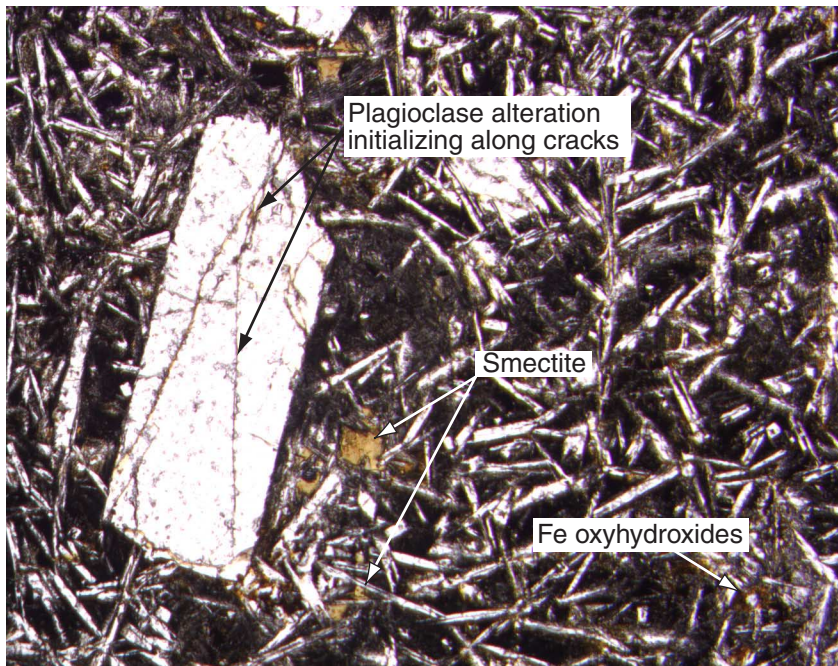


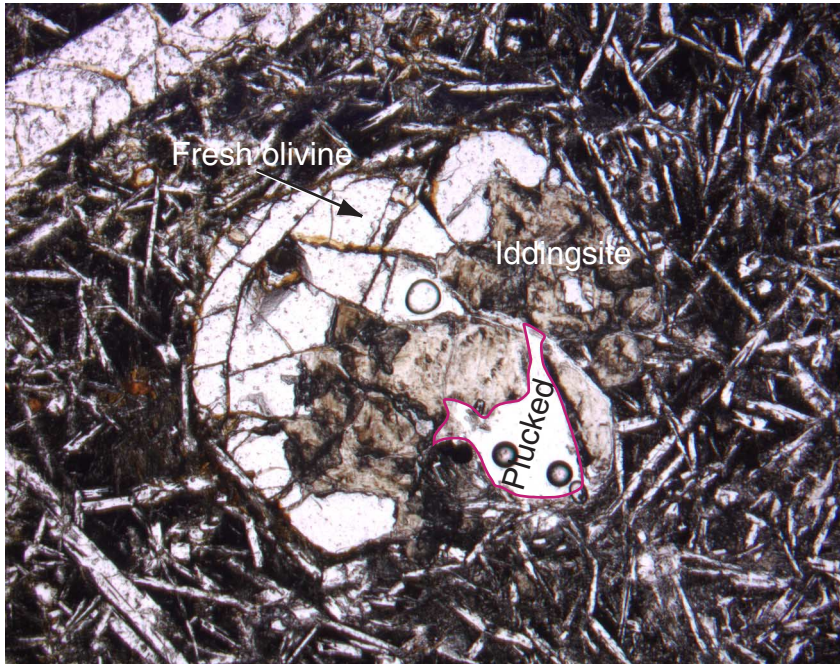
Figure F6. Photomicrograph in plane-polarized light of Sample 187-1156A-2R-1, 8–12 cm (see “[Site 1156 Thin Sections](#),” p. 22), showing ~1% smectite and Fe oxyhydroxide replacement of the groundmass in this basalt. Note the initial stages of alteration along cracks within the plagioclase phenocryst.



2 mm



Figure F7. Photomicrograph in plane-polarized light of Sample 187-1156A-2R-1, 8–12 cm (see “Site 1156 Thin Sections,” p. 22), showing a partly (50%) iddingsitized olivine phenocryst.



2 mm

Figure F8. Photograph of interval 187-1156A-2R-2W, 58–65 cm, showing crosscutting relations between first- and second-generation micritic calcite with respect to the alteration halo in the lower basalt clast (see “Unit 1,” p. 3, in “Igneous Petrology”). Note the relatively fresh angular basalt clasts surrounded by second-generation micritic calcite, as well as the light colored, bleached-white palagonite surrounded by fresh glass. P = rounded yellowish orange palagonite clasts. The triangular vug is filled with third-generation sparry calcite.

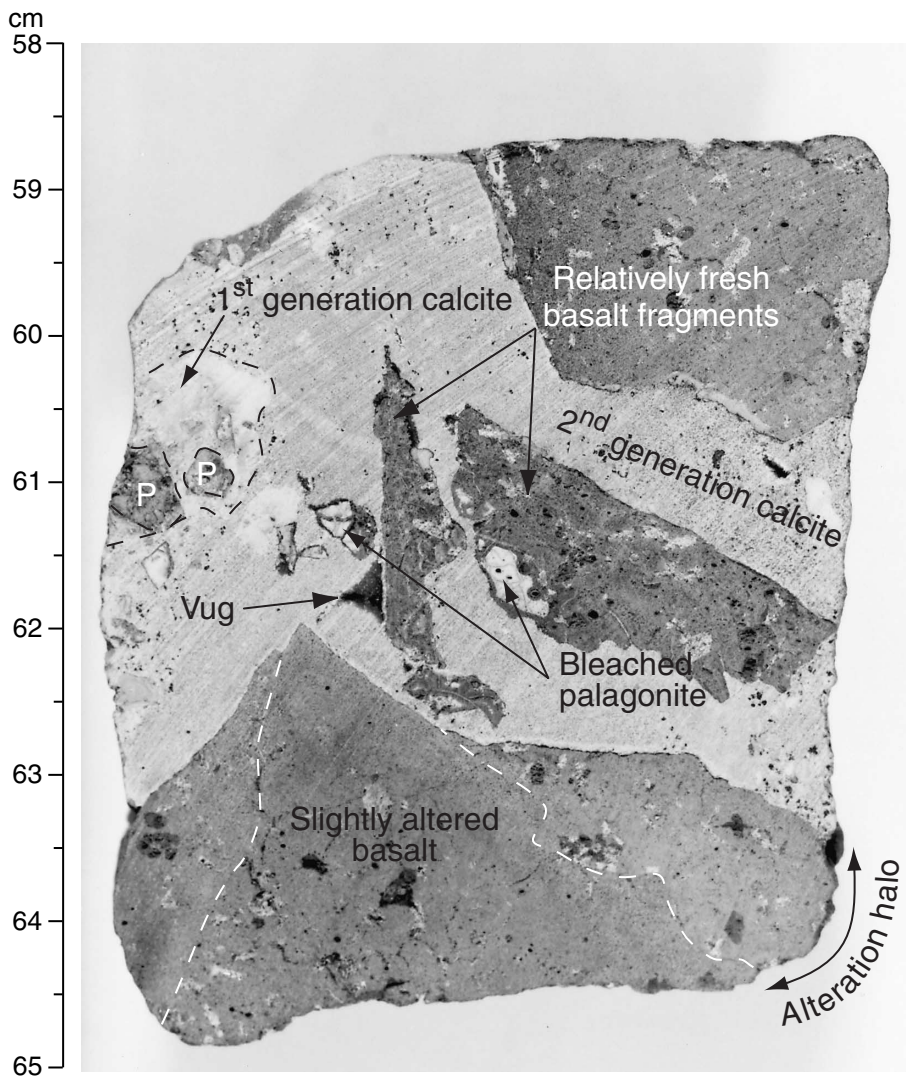


Figure F10. Photograph of interval 187-1156A-2R-1, 67–72 cm, clasts of (1) first-generation calcite, (2) glass surrounded by first-generation calcite, and (3) altered basalt with a bleached palagonite margin, all surrounded by second-generation calcite. Note the constant-thickness palagonitization rims surrounding the glass fragments.

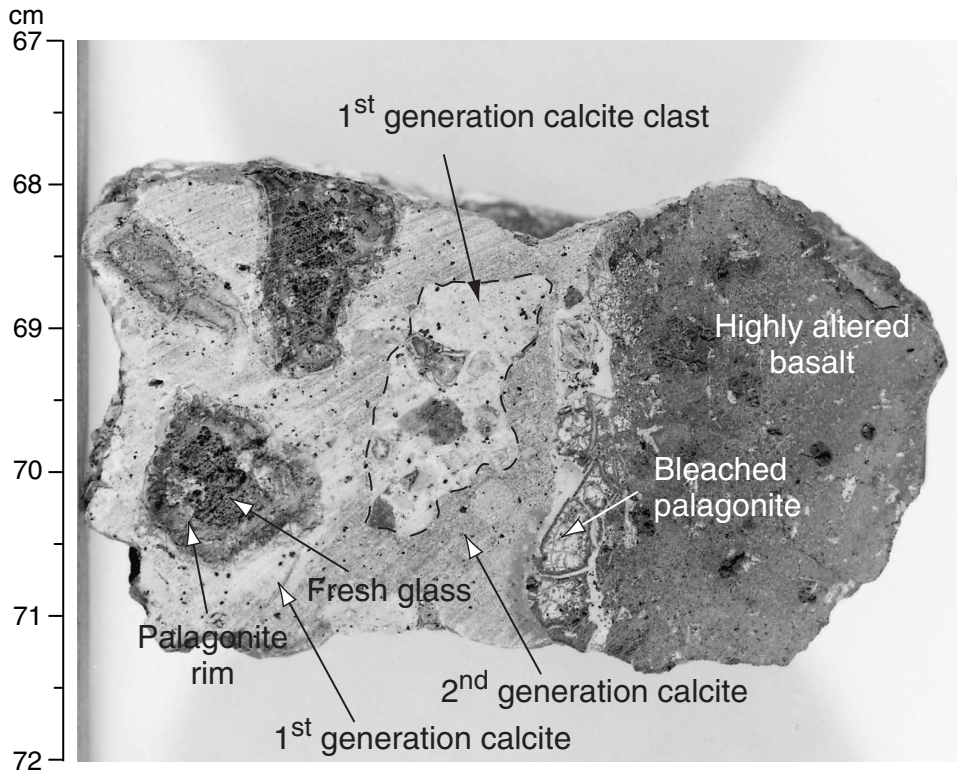


Figure F11. Photograph of interval 187-1156A-3R-1, 102–110 cm, showing perpendicular calcite veins. The narrower vein is oriented orthogonally to the glassy margin and surrounded by an alteration halo. Note the equally wide halo on the closed fracture midway up the left side.

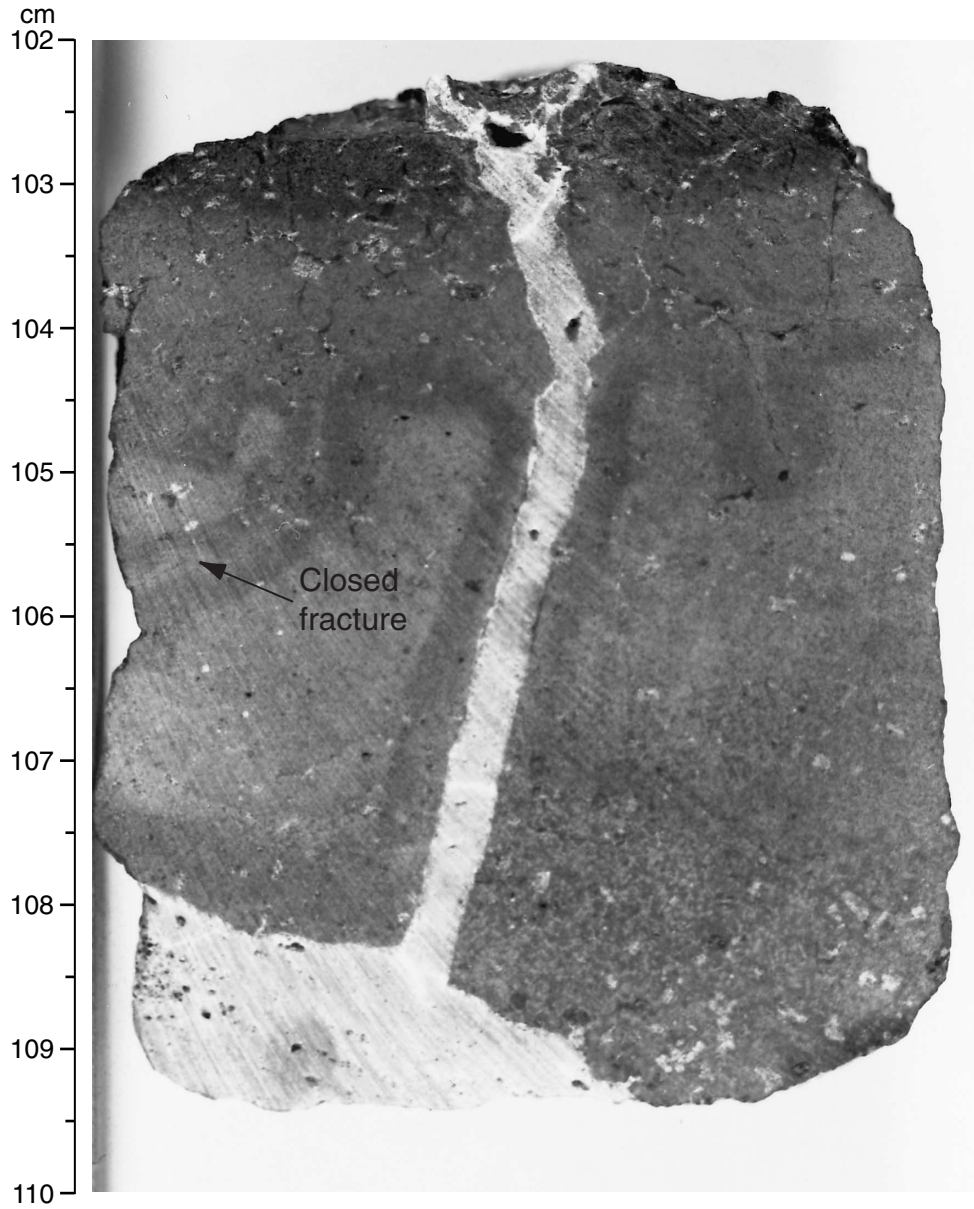


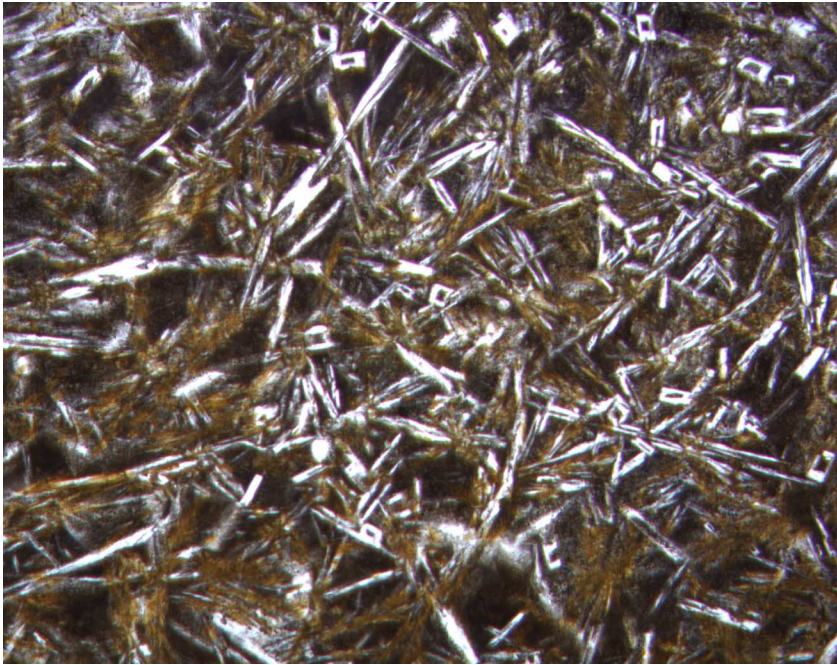
Figure F12. Photomicrograph in plane-polarized light of Sample 187-1156A-3R-1, 5–9 cm (see “[Site 1156 Thin Sections](#),” p. 25), showing plagioclase phenocryst with iron staining along fractures.



1.0 mm



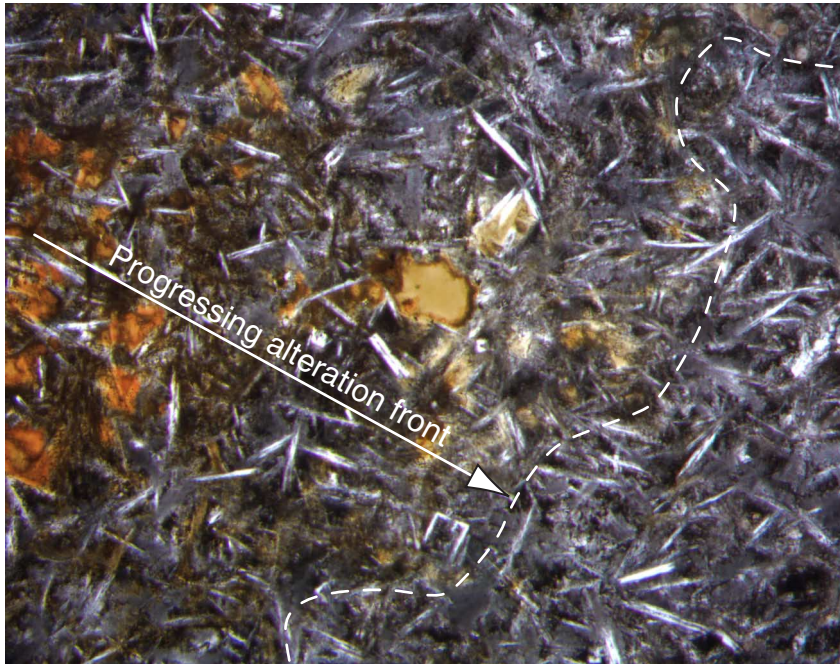
Figure F13. Photomicrograph in plane-polarized light of Sample 187-1156A-3R-1, 5–9 cm (see “[Site 1156 Thin Sections](#),” p. 25), showing ~30% alteration of groundmass clinopyroxene, plagioclase, and devitrified interstitial glass to smectite and Fe oxyhydroxide.



1.0 mm



Figure F14. Photomicrograph of Sample 187-1156A-2R-3, 129–133 cm (see “Site 1156 Thin Sections,” p. 24), showing the transition zone from partial smectite and Fe oxyhydroxide groundmass replacement to virtually unaltered groundmass at an alteration halo boundary.



1 mm



Figure F15. Relative abundances of basalt, pink micritic (first-generation) calcite, and light gray micritic (second-generation) calcite in breccia from Hole 1156A (Sections 187-1156A-2R-1 through 2R-3).

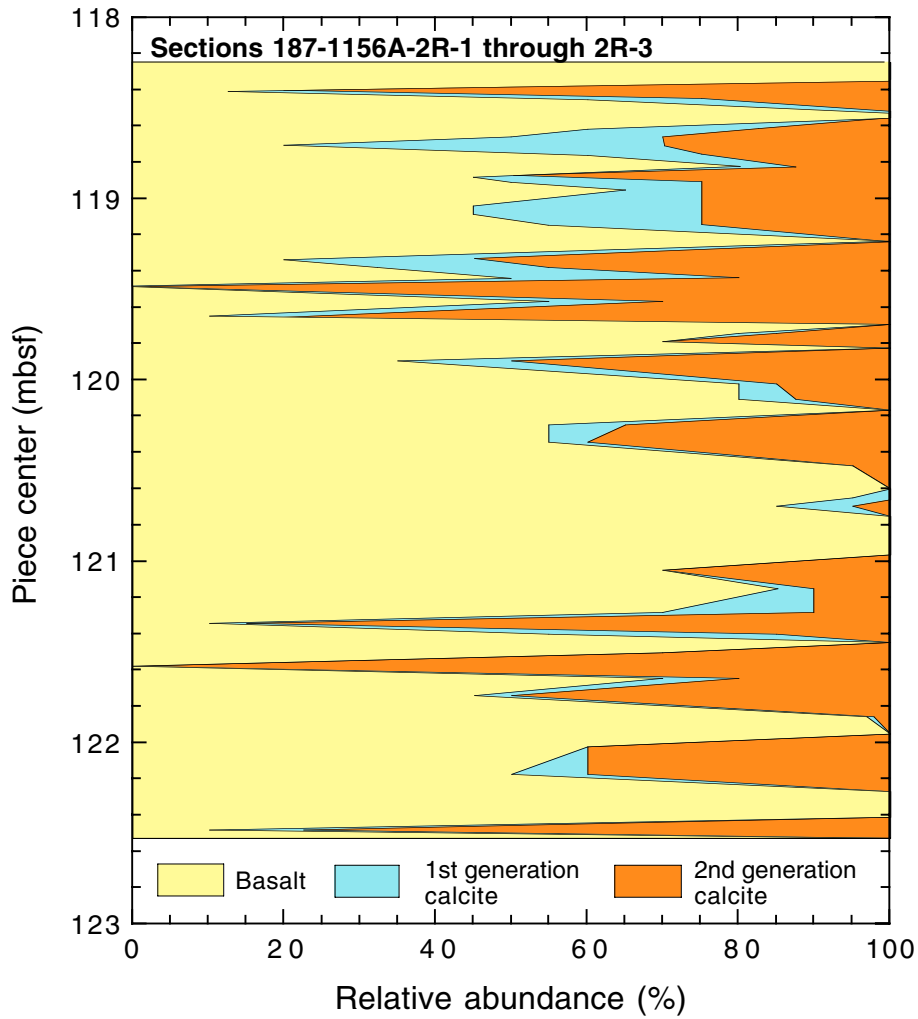


Figure F16. Fragments of basalt with attached pink micritic (first-generation) calcite and palagonite in light gray (second-generation) calcite can be fitted together in places, suggesting little or no displacement during brecciation (Section 187-1156A-1R-1, 113–119 cm).

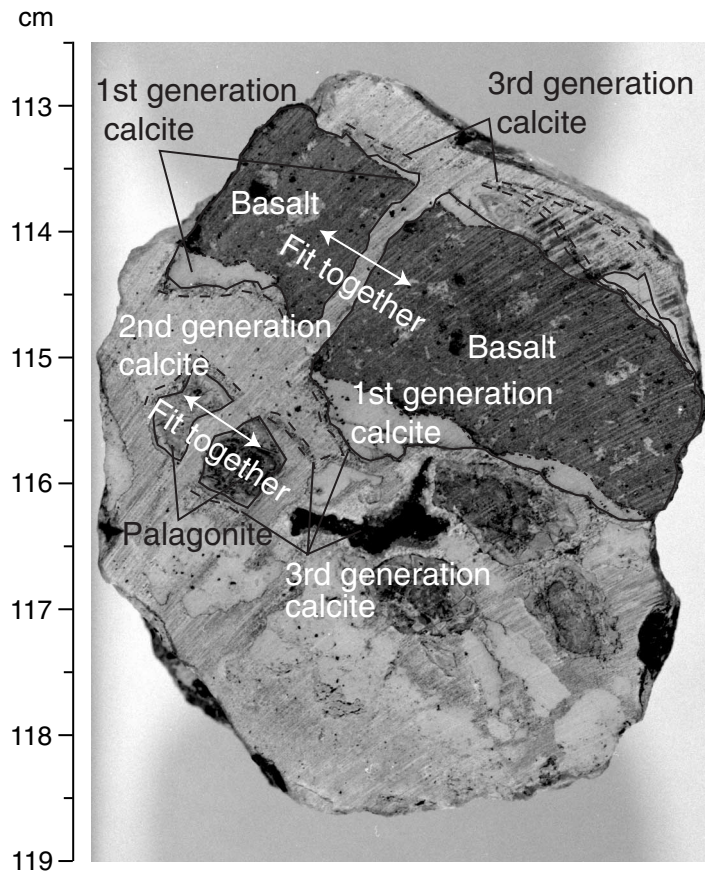


Figure F17. A plot of fracture + vein density (N/m = number per meter) calculated for each section from Site 1156. The horizontal thick line and associated number represent the average for each hole.

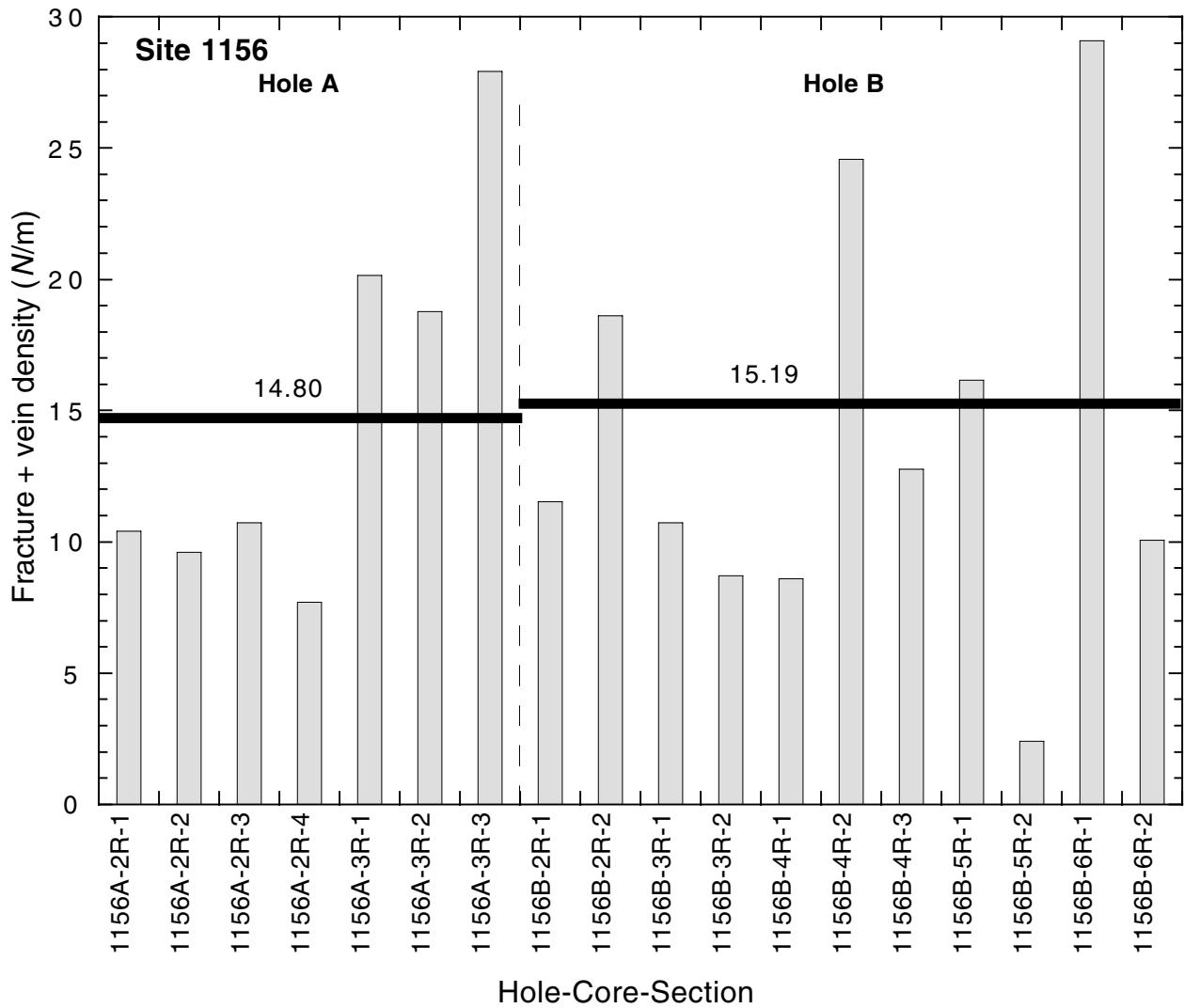


Figure F18. Core table photos of (A) Core 187-1156A-2R and (B) Core 187-1156-3R. Core 2R is a basaltic breccia with abundant matrix, whereas Core 3R is almost exclusively basalt fragments.

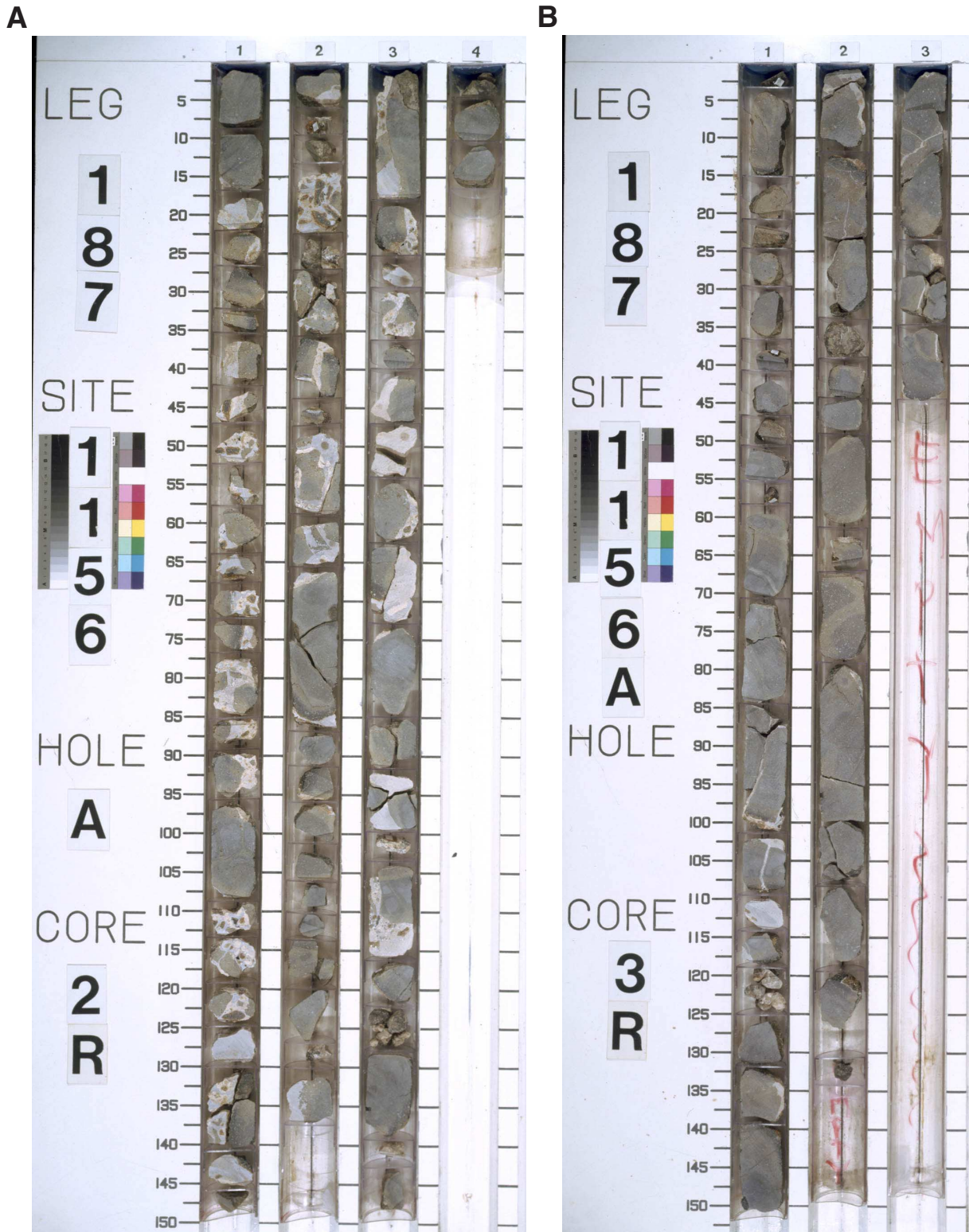


Figure F19. Seismic profile from *R/V Melville* cruise Sojourner 5 (04:00–05:59 Universal Time Coordinated, 24 February 1997) crossing the location of prospectus site AAD-34a. Shots are labeled every 15 min. Site 1156 is near shotpoint 270. Data have been filtered (1, 30, 375, 400), stacked, and migrated (90%).

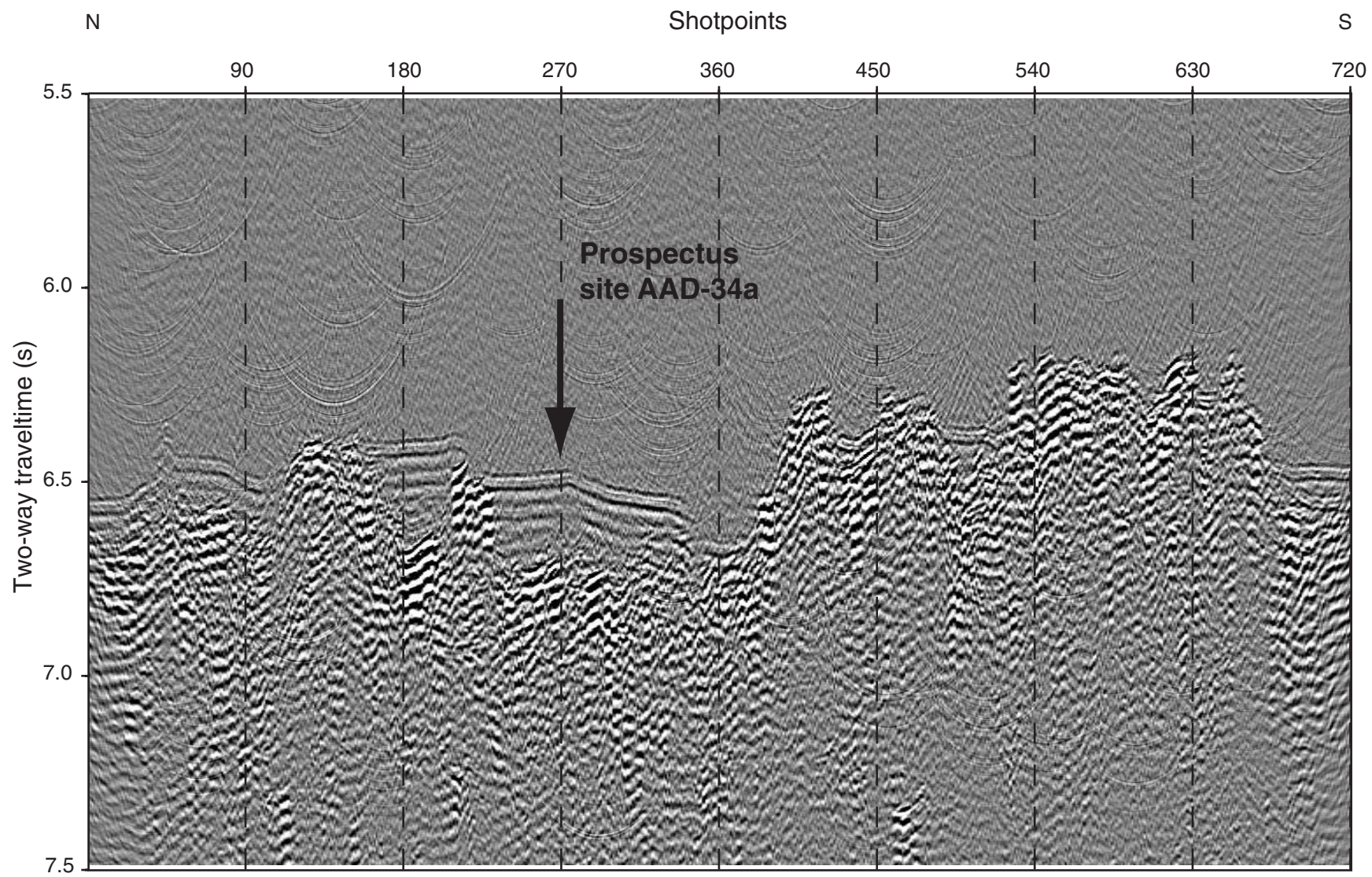


Figure F20. Part of the track of the *JOIDES Resolution* 3.5-kHz precision depth recorder west-to-east survey line S4. Holes 1156A and 1156B (solid circles) are ~400 and 600 m north of prospectus site AAD-34a (open circle).

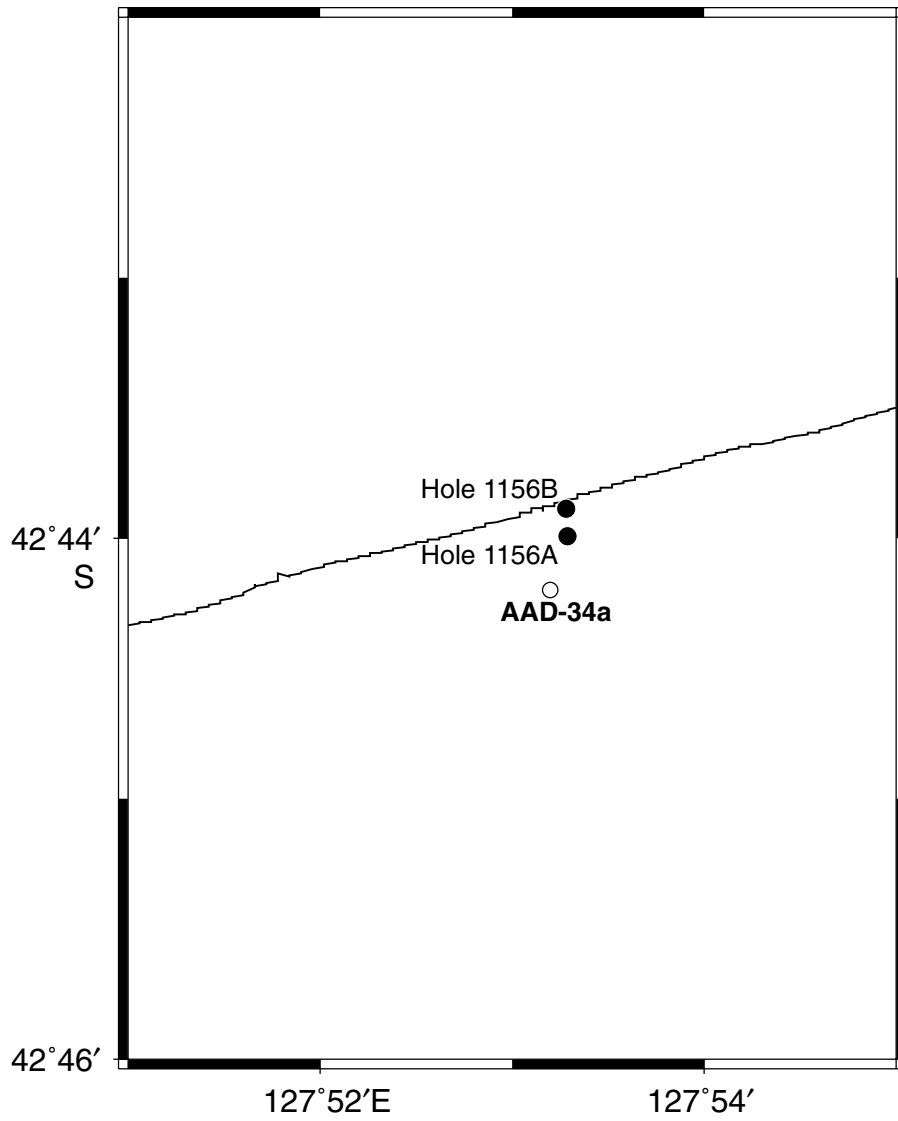


Figure F21. Major element compositions vs. MgO of basalts from Holes 1156A and 1156B compared with Southeast Indian Ridge glasses from Segment B5. Only the average X-ray fluorescence (XRF) or ICP-AES analyses reported in Table T3, p. 38, are plotted. XRF and ICP-AES data for splits of a single whole-rock powder are shown on all plots; two points represent each type of analysis for one sample.

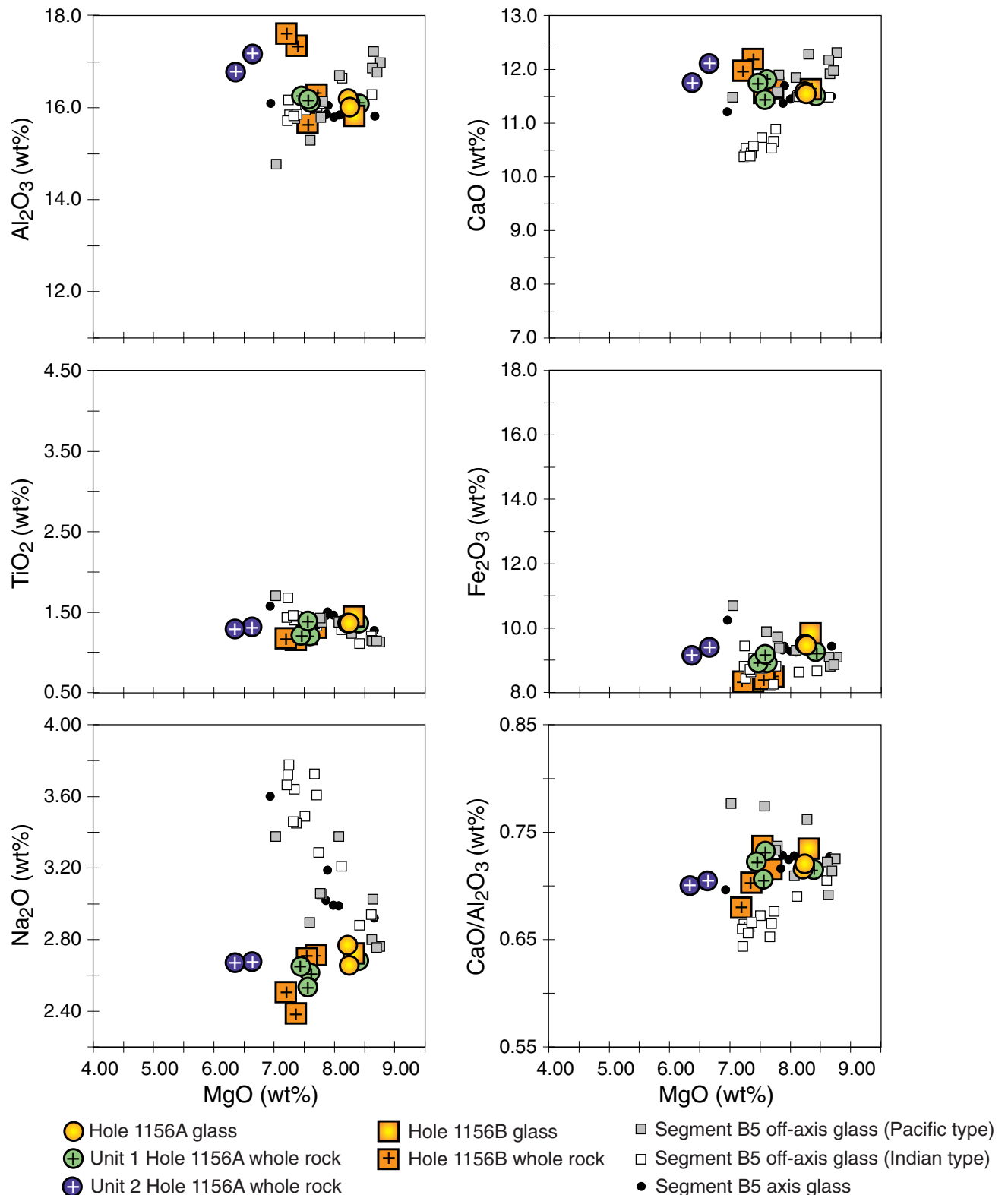


Figure F22. Trace element compositions vs. MgO of basalts from Holes 1156A and 1156B compared with Southeast Indian Ridge glasses from Segment B5.

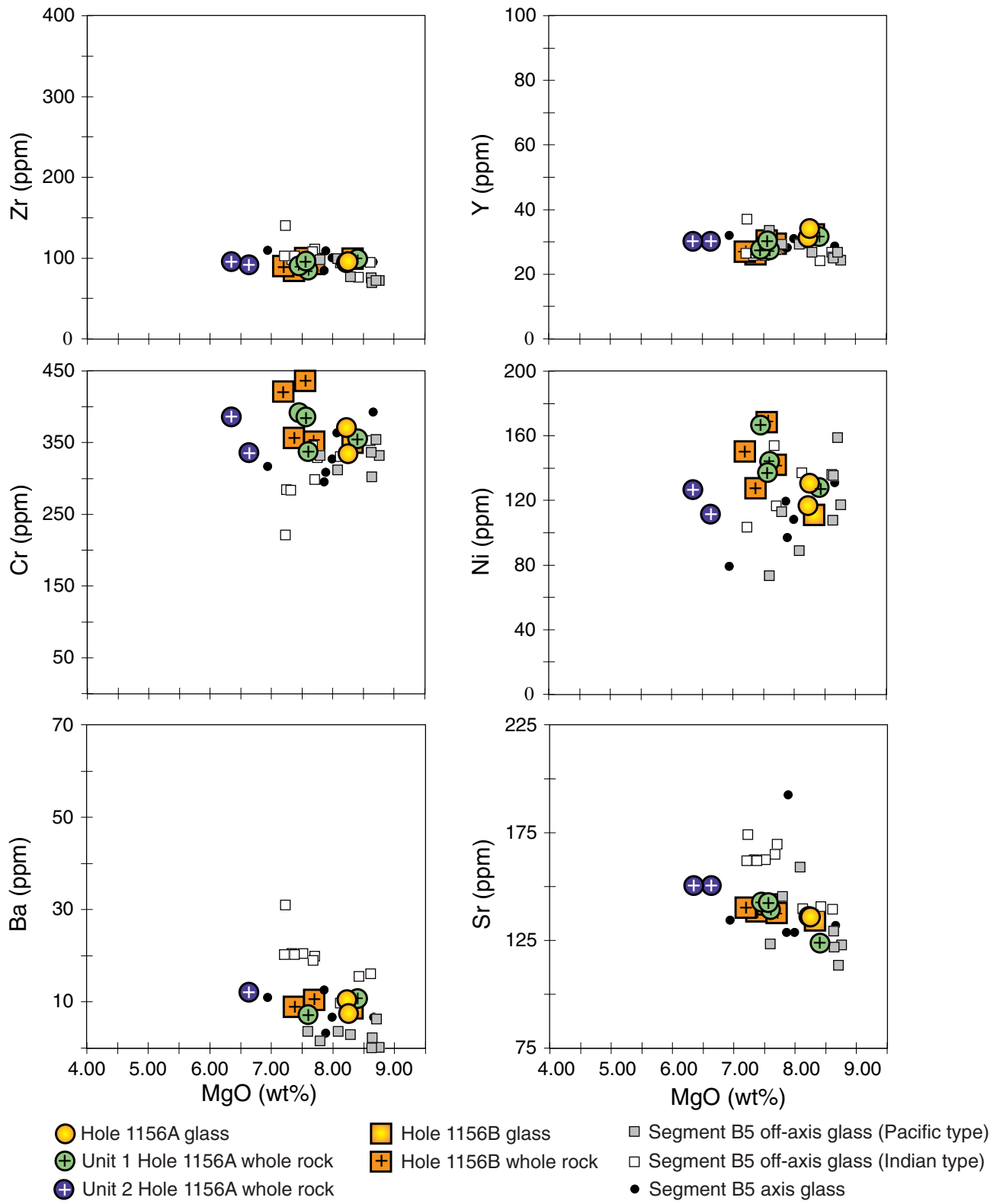


Figure F23. A. Variations of Zr/Ba vs. Ba for Holes 1156A and 1156B glass and whole rocks compared with Indian- and Pacific-type mid-ocean-ridge basalt (MORB) fields defined by zero-age Southeast Indian Ridge (SEIR) lavas dredged between 123°E and 133°E. B. Variations of Na₂O/TiO₂ vs. MgO for Holes 1156A and 1156B glass and whole rocks compared with Indian- and Pacific-type MORB fields defined by zero-age SEIR lavas dredged between 123°E and 133°E. Dashed line separates Indian- and Pacific-type zero-age SEIR basalt glass.

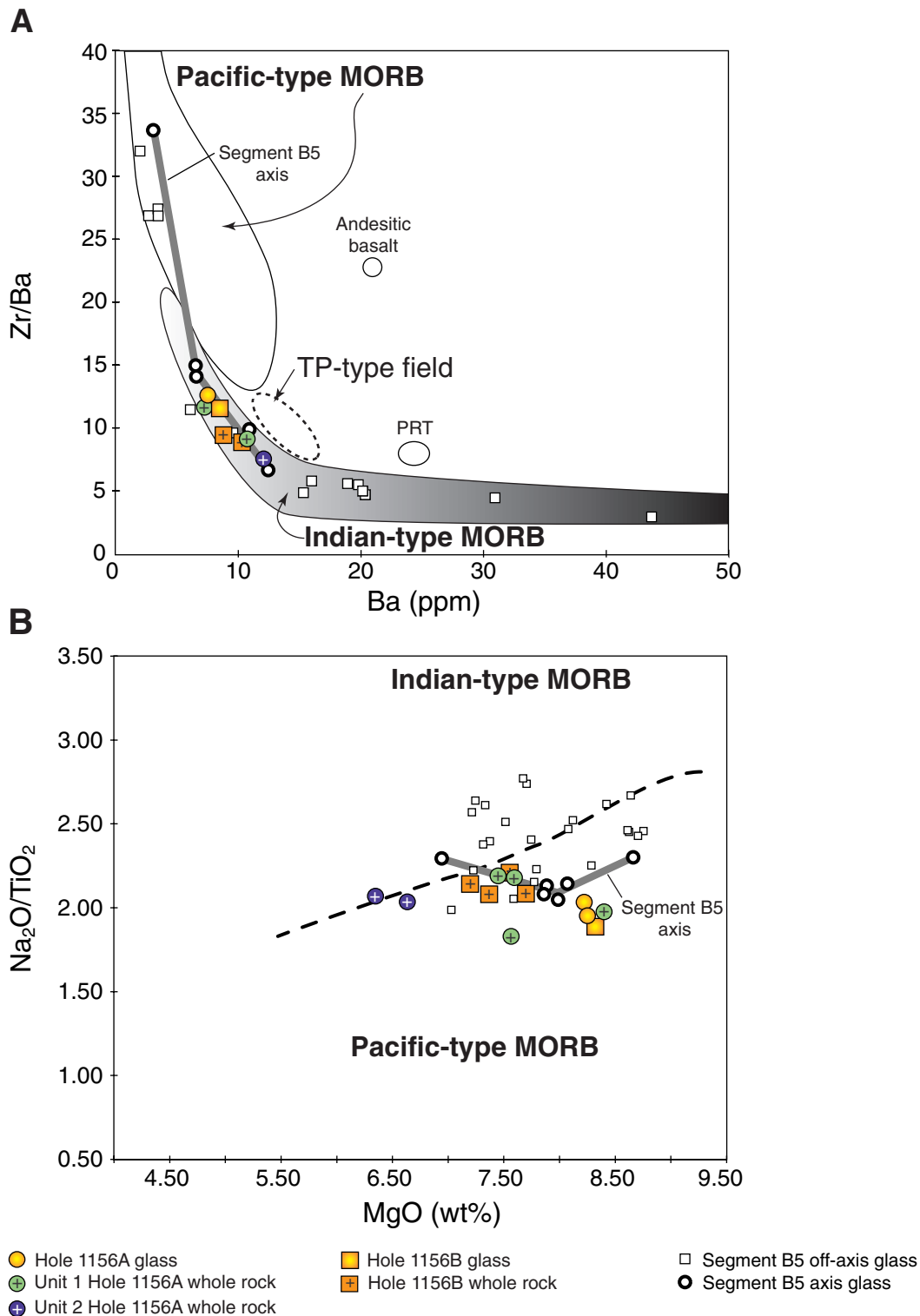


Table T1. Coring summary, Site 1156.

Hole 1156A

Latitude: 42°43.9933'S
 Longitude: 127°53.2912'E
 Time on hole: 1515 hr, 9 Dec 99–1500 hr, 10 Dec 99 (23.75 hr)
 Time on site: 1515 hr, 9 Dec 99–0900 hr, 12 Dec 99 (65.75 hr)
 Seafloor (drill-pipe measurement from rig floor, mbrf): 4878.4
 Distance between rig floor and sea level (m): 11.1
 Water depth (drill-pipe measurement from sea level, m): 4867.3
 Total depth (from rig floor, mbrf): 5008.0
 Total penetration (mbsf): 129.6
 Total length of cored section (m): 11.4
 Total length of drilled intervals (m): 118.2
 Total core recovered (m): 6.3
 Core recovery (%): 55.3
 Total number of cores: 3
 Total number of drilled cores: 1

Hole 1156B

Latitude: 42°43.8870'S
 Longitude: 127°53.2827'E
 Time on hole: 1500 hr, 10 Dec 99–0900 hr, 12 Dec 99 (42.0 hr)
 Seafloor (drill-pipe measurement from rig floor, mbrf): 4878.4
 Distance between rig floor and sea level (m): 11.1
 Water depth (drill-pipe measurement from sea level, m): 4867.3
 Total depth (from rig floor, mbrf): 5093.6
 Total penetration (mbsf): 215.2
 Total length of cored section (m): 33.6
 Total length of drilled intervals (m): 181.6
 Total core recovered (m): 9.92
 Core recovery (%): 29.5
 Total number of cores: 5
 Total number of drilled cores: 1

Core	Date (Dec 1999)	Ship local time	Depth (mbsf)		Length (m)		Recovery (%)	Comment
			Top	Bottom	Cored	Recovered		
187-1156A-								
1W	10	0430	0.0	118.2	118.2	0.00	N/A	
2R	10	0800	118.2	124.6	6.4	3.50	54.7	Whirl-Pak
3R	10	1110	124.6	129.6	5.0	2.80	56.0	
				Cored:	11.4	6.30	55.3	
				Drilled:	118.2			
				Total:	129.6			
187-1156B-								
1W	10	2225	0.0	181.6	181.6	2.32	N/A	
2R	11	0150	181.6	187.4	5.8	1.29	22.2	Whirl-Pak
3R	11	0520	187.4	196.8	9.4	1.81	19.3	
4R	11	1025	196.8	205.9	9.1	2.88	31.6	Liner destroyed
5R	11	1735	205.9	210.2	4.3	1.69	39.3	No liner
6R	11	2340	210.2	215.2	5.0	2.25	45.0	No liner
				Cored:	33.6	9.92	29.5	
				Drilled:	181.6			
				Total:	215.2			

Notes: N/A = not applicable. This table is also available in [ASCII](#) format.

Table T2. Rock samples incubated for enrichment cultures and prepared for DNA analysis and electron microscope studies and microspheres evaluated for contamination studies.

Core	Depth (mbsf)	Sample type	Enrichment cultures				DNA analysis		SEM/TEM samples	Microspheres†	
			Anaerobic	Aerobic	Microcosm*	High pressure	Wash	Fixed	Air dried	Exterior	Interior
187-1156A-3R	124.6-129.6	Chilled margin	1	1	1 Mn	X	X	X	X	Yes	Yes
187-1156B-2R	181.6-187.4	Chilled margin	9	3	1 Mn + 1 Fe/S	X	X	X	X	Yes	Yes
5R	205.9-210.2	Fine-grained basalt	9	3		X	X	X	X		
6R	210.2-215.2	Chilled margin	5	3	1 Fe/S	X	X	X	X		

Notes: * = microcosm for iron and sulfur (Fe/S) or manganese (Mn) redox cycles; SEM = scanning electron microscope; TEM = transmission electron microscopy; † = contamination test; X = samples prepared on board. This table is also available in [ASCII](#) format.

Table T3. Glass and whole-rock major and trace element compositions of basalts, Hole 1156A. (See table notes. Continued on next page.)

Core, section:	Hole 1156A																	
	2R-1	2R-1	2R-1	2R-1	2R-3	2R-3	2R-3	2R-3	2R-3	2R-3	2R-3	3R-1	3R-1	3R-1	3R-2	3R-2	3R-2	3R-2
Interval (cm):	8-12	8-12	8-12	8-12	129-133	129-133	129-133	129-133	133-138	133-138	133-138	102-109	102-109	102-109	73-77	73-77	73-77	73-77
Depth (mbsf):	118.28	118.28	118.28	118.28	122.35	122.35	122.35	122.35	122.39	122.39	122.39	125.62	125.62	125.62	126.83	126.83	126.83	126.83
Piece:	2	2	2	2	17	17	17	17	17	17	17	15	15	15	8	8	8	8
Unit:	1	1	1	1	1	1	1	1	1	1	1	2	2	2	2	2	2	2
Analysis:	XRF	XRF	ICP	ICP	XRF	XRF	ICP	XRF	XRF	ICP	ICP							
Rock type:	Moderately plagioclase-olivine phyric basalt				Moderately plagioclase-olivine phyric basalt				Glass	Glass	Glass	Glass	Glass	Glass	Moderately plagioclase-olivine phyric basalt			
Major element (wt%)																		
SiO ₂	49.16	47.89	49.71	49.58	49.58	49.21	51.08	52.18	50.33	50.96	52.38	49.58	50.34	51.20	47.96	48.03	50.42	50.52
TiO ₂	1.25	1.17	1.20	1.20	1.46	1.31	1.36	1.36	1.36	1.37	1.36	1.34	1.37	1.37	1.28	1.30	1.30	1.33
Al ₂ O ₃	16.43	16.12	16.33	15.96	16.46	15.95	16.00	16.21	16.35	16.28	16.01	16.15	16.09	15.88	16.80	16.80	17.07	17.32
Fe ₂ O ₃	9.00	8.82	8.98	8.82	9.16	9.18	9.18	9.34	9.38	9.49	9.60	9.37	9.45	9.54	9.15	9.13	9.42	9.38
MnO	0.15	0.13	0.15	0.15	0.17	0.15	0.16	0.16	0.16	0.16	0.16	0.15	0.16	0.16	0.15	0.15	0.16	0.16
MgO	7.58	7.32	7.54	7.66	7.60	7.53	8.43	8.38	8.14	8.26	8.28	8.14	8.29	8.32	6.37	6.33	6.68	6.60
CaO	11.83	11.66	11.81	11.81	11.42	11.45	11.50	11.51	11.50	11.48	11.79	11.48	11.43	11.72	11.79	11.72	12.10	12.12
Na ₂ O	2.69	2.61	2.66	2.57	2.41	2.66	2.68	2.68	2.75	2.75	2.81	2.43	2.74	2.80	2.63	2.71	2.69	2.66
K ₂ O	0.34	0.32	0.29	0.31	0.41	0.38	0.10	0.10	0.12	0.11	0.11	0.11	0.11	0.10	0.20	0.20	0.17	0.17
P ₂ O ₅	0.12	0.12	0.14	0.14	0.12	0.12	0.16	0.15	0.15	0.15	0.14	0.15	0.14	0.14	0.13	0.13	0.16	0.14
LOI	1.19	1.19			0.97	0.97									0.86	0.86		
CO ₂																		
H ₂ O																		
Total:	99.74	97.35	98.82	98.19	99.76	98.91	100.66	102.06	100.23	101.01	102.65	98.90	100.11	101.22	97.32	97.36	100.16	100.39
Trace element (ppm)																		
Nb	6				6										6			
Zr	91		86	85	96		99	99	96	94	94	96	95	97	96		92	91
Y	28		28	27	30		32	32	32	31	32	34	34	35	30		30	31
Sr	143		140	139	143		124	123	136	135	137	135	136	137	151		149	152
Rb	7				8										1			
Zn	70				74										80			
Cu	63				64										62			
Ni	167		144	145	137		125	131	115	116	120	129	132	131	127		112	111
Cr	392		334	342	386		352	360	365	365	382	322	335	347	386		346	327
V	244				250										263			
Ce	25				25										30			
Ba			7	7			11	11	10	11	11	8	8	8			12	12
Sc			32	31			34	35	36	36	37	36	36	36			34	36

Table T3 (continued).

Core, section:	Hole 1156B											
	2R-1	2R-1	2R-1	2R-1	4R-1	4R-1	4R-1	5R-1	5R-1	5R-1	5R-1	
Interval (cm):	62-65	62-65	62-65	62-65	102-107	102-107	102-107	75-79	75-79	75-79	75-79	
Depth (mbsf):	182.22	182.22	182.22	182.22	197.82	197.82	197.82	206.65	206.65	206.65	206.65	
Piece:	9	9	9	9	20	20	20	7	7	7	7	
Unit:	1	1	1	1	1	1	1	1	1	1	1	
Analysis:	XRF	XRF	ICP	ICP	ICP	ICP	ICP	XRF	XRF	ICP	ICP	
Rock type:	Moderately plagioclase-olivine phyric basalt				Moderately plagioclase-olivine phyric basalt			Moderately plagioclase-olivine phyric basalt				
Major element (wt%)												
SiO ₂	48.17	47.98	48.75	50.13	50.72	51.90	51.72	48.91	48.47	49.56	50.30	
TiO ₂	1.17	1.17	1.14	1.15	1.44	1.46	1.43	1.25	1.19	1.30	1.30	
Al ₂ O ₃	17.65	17.61	17.54	17.19	15.99	15.83	15.70	15.82	15.57	16.22	16.38	
Fe ₂ O ₃	8.35	8.28	8.38	8.25	9.74	9.92	9.80	8.48	8.32	8.37	8.57	
MnO	0.13	0.13	0.13	0.13	0.16	0.17	0.17	0.13	0.12	0.14	0.15	
MgO	7.24	7.16	7.35	7.39	8.39	8.30	8.29	7.62	7.49	7.65	7.75	
CaO	11.99	11.95	12.21	12.17	11.50	11.68	11.68	11.56	11.55	11.61	11.67	
Na ₂ O	2.50	2.51	2.39	2.38	2.69	2.79	2.68	2.72	2.67	2.66	2.76	
K ₂ O	0.22	0.22	0.19	0.19	0.13	0.12	0.12	0.16	0.15	0.16	0.17	
P ₂ O ₅	0.12	0.12	0.14	0.14	0.16	0.16	0.16	0.13	0.13	0.13	0.14	
LOI	0.44	0.44										
CO ₂												
H ₂ O												
Total:	97.98	97.57	98.22	99.14	100.91	102.31	101.74	96.78	95.66	97.81	99.19	
Trace element (ppm)												
Nb	6							6				
Zr	90		85	83	99	100	99	100		91	94	
Y	27		26	26	32	32	33	30		29	30	
Sr	140		138	139	134	133	135	142		136	139	
Rb	3							2				
Zn	66							72				
Cu	61							65				
Ni	150		127	128	108	114	111	168		142	142	
Cr	421		356	357	336	355	356	436		346	356	
V	241							254				
Ce	28							31				
Ba			9	9	9	9	8			10	10	
Sc			30	30	38	38	38			35	36	

Notes: LOI = loss on ignition. This table is also available in [ASCII](#) format.